DESIGN OF AN ELECTRO-THERMAL NANO- AND MICROSATELLITE PROPULSION SYSTEM

THESIS

James H. Founds, Captain, USSF

AFIT-ENY-MS-22-M-291

DEPARTMENT OF THE AIR FORCE
AIR UNIVERSITY

AIR FORCE INSTITUTE OF TECHNOLOGY

Wright-Patterson Air Force Base, Ohio

AFIT-ENY-MS-22-M-291

DESIGN OF AN ELECTRO-THERMAL NANO- AND MICROSATELLITE PROPULSION SYSTEM

THESIS

Presented to the Faculty

Department of Aeronautics and Astronautics

Graduate School of Engineering and Management

Air Force Institute of Technology

Air University

Air Education and Training Command

In Partial Fulfillment of the Requirements for the

Degree of Master of Science in Aeronautical Engineering

James H. Founds, BS

Captain, USSF

March 2022

AFIT-ENY-MS-22-M-291

DESIGN OF AN ELECTRO-THERMAL NANO- AND MICROSATELLITE PROPULSION SYSTEM

James H. Founds, BS

Captain, USSF

Committee Membership:

Dr. Carl R. Hartsfield
Chair

Dr. Andrew S. Keys
Member

Maj Daniel S. O'Keefe, PhD
Member

AFIT-ENY-MS-22-M-291

Abstract

This research focused on designing an arcjet system with water as the propellant. Previous research developed a compact, reliable, and safe propellant storage and feed system. The goal of this research is to combine the arcjet with the previous tank to achieve thrust, specific impulse, and Δv characteristics greater than a cold gas or resistojet system. The thruster and propellant tank are less than 1U in volume, non-hazardous, and require less than a kilowatt of power. A simplified analysis of the design predicts thrust and specific impulse greater than can be achieved by cold gas or resistojet thrusters. Testing resulted in pitting and deposition on the electrodes surface raising concerns about the longevity of the system. Electrode degradation reduced the reliability of arc initiation. Resolution to these issues make the system suboptimal for implementation in nano- or microsatellites.

Acknowledgments

I would like to express my sincere appreciation to my faculty advisor, Dr. Carl Hartsfield, for his guidance and support throughout this thesis effort. I will always appreciate his opinions and work done for this project, thank you. I would, also, like to thank my wife for all her support and confidence in me. It would not have been possible without her.

James H. Founds

Table of Contents

List of Figures

Page

List of Tables

Page

DESIGN OF AN ELECTRO-THERMAL NANO- AND MICROSATELLITE PROPULSION SYSTEM

I. Introduction

Background

Small satellites (<600 kgs.) have continued to grow in popularity over the past decade with nano- (1.1-10 kg) and microsatellites (11-200 kg) the majority of small satellites launched, excluding Starlink and OneWeb launches [1]. Nano- and microsatellites can also fall into the category of a CubeSat. CubeSats are categorized by a standardized volume of Us. A "U" is the volume taken of a box that measures 10 cm on each side. CubeSat volumes range from 1U to 12U with masses that range between the nano- and microsatellite categories. Space propulsion for small satellites is an important research area to increase their capabilities. Propulsion enables satellite activities such as changing orbital altitude, making orbit corrections, deorbiting on command, flying in formation, constellation deployment, or interplanetary missions [2]. Thrust and specific impulse are succinct metrics that determine a system's ability to complete the activities listed above.

NASA categorizes propulsion systems as either chemical, electric, or propellant-less [3]. Chemical propulsion system's thrust and specific impulse range from micro-Newtons to hundreds of Newtons and tens of seconds to hundreds of seconds of specific impulse [2], [3]. Electric propulsion systems range from micro-Newtons to hundreds of milli-Newtons and tens of seconds to thousands of seconds of specific impulse [2], [3]. Propellant-less systems have yet to significantly demonstrate their capabilities. Current chemical propulsion systems are defined by their use of different propellants.

Monopropellants, cold/warm gas thrusters, and solid motors are common examples of chemical propulsion systems. Hydrazine, a common monopropellant, is a toxic and corrosive chemical that requires specific additional safety measures during integration. Other monopropellants are not as toxic or dangerous but sacrifice performance. Cold gas thrusters reduce dangers posed by the propellant but at the cost of thrust and specific impulse. Cold gas thrusters are capable of producing thrust between 0.01 and 70 milli-Newtons and specific impulse between 40-100 seconds [3]. Solid motors provide large amounts of thrust and moderate specific impulse at the expense of single use applications. Electrospray, gridded ion, Hall-effect, pulsed plasma, vacuum arc, ambipolar, and electrothermal systems make up the demonstrated electric propulsion systems. Electrospray systems provide thrust values that range from micro-Newtons to milli-Newtons and specific impulse that range from hundreds to thousands of seconds [2]–[4]. Gridded ion thrusters provide micro-Newtons to tens of Newtons of thrust and several thousands of seconds of specific impulse. Hall effect thrusters provide similar thrust to ion engines, tens of milli-Newtons, but at lower specific impulse values, hundreds to thousands of seconds. Resistojet, arcjet, and electrodeless systems subdivide the electrothermal category. These systems thrust values range from several milli-Newtons to hundreds of milli-Newtons and tens to hundreds of seconds of specific impulse.

Each of these systems have inherent advantages and disadvantages relative to a specific mission. Microsatellites rarely have the luxury of being the sole mission for a given launch vehicle. These systems are often a secondary payload to larger satellites. The desire then is for a compact, reliable, and safe propulsion system. Cold/Warm gas and electrothermal systems can potentially be operated with harmless propellants.

Commonly used propellants include water, nitrogen, argon, and refrigerants. Gas systems are highly reliable requiring only a valve to release the pressurized gas. Pressurized tanks pose a potential hazard to the integrated payload if ruptured. Ideally the system would not be under pressure during payload integration and then pressurized once on station. Such a system would require minimal augmentation to increase its thrust and specific impulse capabilities. A resistojet requires minimal additional hardware and could even be run off spacecraft bus power. An arcjet would require a more complex power processing unit than that of a resistojet. Arc ignition requires high voltages and would need to be adjusted to maintain the arc. If feasible, arcjets, increase the available specific impulse and thrust. Hall thrusters appear to offer the best performance for electrical propulsion systems in terms of thrust and specific impulse [2]. Scaling the systems down to 1U and 2U sizes introduces inefficiencies that must be compensated for with more complex power processing units. Arcjets offer a middle ground of performance for a compact, reliable, and safe propulsion system for microsatellites.

Problem Statement

Current microsatellites propulsion systems either have low amounts of thrust and specific impulse or else utilize hazardous chemical that pose potential risks to other payloads. Previous research developed a compact CubeSat propulsion system with a resistojet as the primary propulsion system. Designing an arcjet system with water as the propellant may provide greater specific impulse and thrust resulting in increased ΔV, but what costs will be incurred?

Research Objectives/Questions/Hypotheses

The objective of this research is to develop and test a prototype, water-fueled arcjet propulsion system for use in a 1U form factor for CubeSat missions. Is the system able to achieve greater specific impulse and thrust without requiring power in excess of 200W?

Research Focus

The focus of the research is on the feasibility of a 3D printed inconel & tungsten arcjet utilizing water as the propellant for use as a CubeSat propulsion system. Two different tungsten cathodes were chosen for comparison of the ability to strike and maintain the arc in vacuum.

Investigative Questions

What is the difference between the theoretically estimated and experimental thrust and specific impulse for such a system? Does the increased specific impulse of an arcjet system result in a useable payload mass fraction given the additional complexity, size, weight, and power?

II. Literature Review

Chapter Overview

The purpose of this chapter is to develop an understanding of the metrics used to compare spacecraft propulsion systems. Thrust and specific impulse are the basic metrics to compare of the different systems. Comparing the underlying mechanisms for different propulsion systems allows for estimates of theoretical performance. An arcjet may produce better specific impulse than either a cold gas thruster or a resistojet, but the increased complexity of the power processing unit may be worse than simply increasing the propellant mass for simple systems. Different capabilities optimize the maximum payload mass given different mission requirements. A propulsion system with a high specific impulse is optimized for different situations than a system with a high thrust but low specific impulse.

Last is a review of the support system necessary to support an arcjet. Support equipment consists of the electrical processing to change bus and battery voltage to a high voltage for arc ignition. Battery capacity influences the time required to perform different maneuvers. Understanding the trade space available if solar panels are available is introduced at the end.

Propulsion

Thrust, Specific Impulse, and Velocity Change

Rocket propulsion is the generation of thrust as a reaction to ejecting material opposite to the direction of desired thrust. The material or propellant is a working fluid

stored within the rocket. The mass of ejected material is proportional to the thrust generated. Ejecting propellant at a higher velocity also increases the thrust produced. The result is that thrust is a change in momentum over time. A simple derivation is shown below.

$$\sum F = \frac{d(m \cdot v)}{dt} = \frac{dm}{dt} \cdot v + m \cdot \frac{dv}{dt} \quad (1)$$

This equation illustrates the statements made earlier. If there are no other forces, then the second term on the right-hand side is the acceleration of the vehicle, the first term on the right-hand side is the momentum thrust of the rocket engine, and the left-hand side is zero. The first term on the right illustrates that expending mass at higher velocities increases thrust. This concept governs all propellant-based propulsion systems. Increasing the average molecular mass of the propellant generally decreases the velocity at which it is ejected. It is more common to utilize lighter propellants that can be accelerated faster out of the rocket. Accelerating the propellant is accomplished by pressurizing and expanding it through a converging-diverging nozzle, also known as a De Laval nozzle.

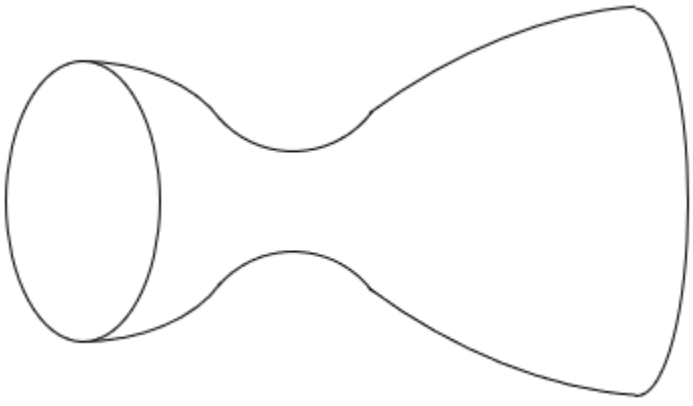

Figure 1. De Laval Nozzle Configuration

Propellant pressure and/or temperature can be increased in order to also increase the system's specific impulse, I_{sp}.

Specific impulse is a measure of the system's ability to convert propellant mass into thrust. Equation 2 illustrates the relationship between thrust and specific impulse [5].

$$I_{sp} = \frac{F}{\dot{m} \cdot g_o} \tag{2}$$

Specific impulse is a ratio of the thrust produced to the product of mass flow and a gravitational constant. Increased thrust for a given mass increases specific impulse. Similarly, a reduced mass flow for a given thrust also increases a rocket's specific impulse. Specific impulse can also be thought of as a ratio of a propellant's exit velocity to the gravitational constant. Modifying equation 2 achieves the following result.

$$I_{sp} = \frac{\dot{m} \cdot u_e}{\dot{m} \cdot g_o} = \frac{u_e}{g_o} \tag{3}$$

As shown, increasing the specific impulse is directly related to increasing the propellant exit velocity. It is important to note that unlike force, specific impulse does not increase with additional propulsion systems. As thrust overall increases so does the overall mass flow. Using the equation shown above this results in the following relationships [5].

$$F_{total} = F_1 + F_2 + F_3 + \cdots \tag{4}$$

$$\dot{m}_{total} = \dot{m}_1 + \dot{m}_2 + \dot{m}_3 + \cdots \tag{5}$$

$$I_{sp_{total}} = \frac{F_{total}}{\dot{m}_{total} * g_o} \tag{6}$$

These relationships show that two similar propulsion systems would have the same specific impulse but would double the thrust produced. To demonstrate, a cold gas system could increase the number of nozzles for a given design. The thrust would

increase as the mass flow increases through the multiple nozzles. Specific impulse remains constant as the mass flow change is directly proportional to the thrust change for a similar system.

Changing position or simply maintaining altitude in orbit requires changing the spacecrafts' velocity. This velocity change is commonly stated as a delta-v, Δv, required. The ideal rocket equation relates delta-v to specific impulse and the initial and final mass of the spacecraft [5].

$$\Delta v = I_{sp} \cdot g_o \cdot \ln \frac{m_o}{m_f} \tag{7}$$

This equation is the basis for performing the ideal flight performance of the system as done in Chapter 4.

Cold Gas, Resistojet, and Arcjet Propulsion Systems

Cold gas, resistojet, and arcjet systems demonstrate a progression of increasing the specific impulse capabilities of a system. Gas propulsion systems use large tanks of a pressurized or saturated propellant that produce thrust when fed through a nozzle. Microelectromechanical valves allow for the thruster portion of the system to be miniaturized to great effect. Pressure within the tanks can range from 300 to 10,000 psi [5], requiring thick tank walls. Combined with the nature of gases having low densities the tanks are also large. In nanosatellites this limits cold gas propulsion use to positioning, formation flight, and attitude control. Demonstrated systems achieved between 2 and 15 meters per second of Δv [6]. This corresponds to the velocity change required to maintain an orbital altitude between 550 and 650 km for a single year at a solar maximum and given a ballistic coefficient of 50 kg/m^2 [7].

Electrothermal systems such as resistojets and arcjets heat the propellant as it passes through the thruster. Heating the propellant increases the exhaust velocity thus raising the specific impulse and thrust.

Resistojets electrically heat propellant by passing the working fluid over a heated surface.

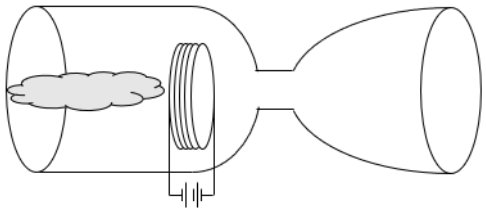

Figure 2 Resistojet

Due to their simplicity, resistojets can be added to cold gas thrusters to increase performance. A variety of configurations exist, such as placing heated wires in the flow path, as shown in Figure 2, or by heating the chamber walls. Resistojets can be easily miniaturized and operate over a wide range of power levels. Typical resistojet specifications for nanosatellites are shown in Table 1.

Table 1 Demonstrated Resistojet Capabilities [3]

Specific Impulse (s)	Thrust (mN)	Required Power (W)	Volume (cm^3)	Mass (kg)
70 - 150	0.5 – 17	10 – 55	300 – 2,600	0.28 – 1.44

Estimated velocity changes for these systems range from 50 to 125 m/s. This provides enough delta-v to counter orbital decay for a year between 450 – 500 km at a solar maximum given a ballistic coefficient of 50 kg/m^2 [7]. This would double a CubeSat's operational life or provide a rapid commanded deorbit capability out to a 500 km altitude [7]. Thermal management of the resistojet should also be considered. Heat inevitably

transfers along structure and propellant connections to the rest of the spacecraft. If not considered during integration, thermal management may problems may arise.

Arcjets improve upon the resistojet's propellant exhaust velocity by heating and constricting the core flow. Ohmic heating generates heat in the propellant as a result of its inherent resistance. Accomplishing this is done through the discharge of an electrical arc between two electrodes as shown in the Figure 3.

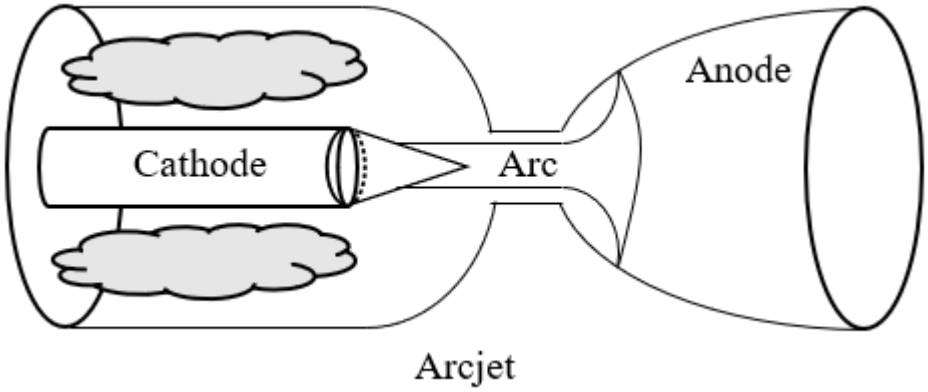

Figure 3 Arcjet

A more complex power processing unit is required for the arcjet compared to cold gas and resistojet systems. This is due to the nature of an electric discharge in the gas. In summary, the voltage and current increase until a breakdown voltage is achieved. Breakdown voltages are a function of the electrode material and geometry, propellant, pressure, and electrode gap distance. Once breakdown is achieved, the voltage drops to a steady gap voltage, while the current can be increased. Over a short amount of time the voltage increases as the cathode heats. At some point the cathode is heated sufficiently that electrons are emitted thermionically. After this point the voltage drops while the resistance in the arc drops to a greater degree. If uncontrolled, high amperages would run through the electrodes possibly damaging or vaporizing the electrodes. Some form of an

electrical ballast is required to prevent a runaway amperage from damaging the system. Due to the added electrical complexity currently, as of 2022, there are no planned or demonstrated arcjet propulsion systems for flight use in CubeSats.

Typical performance values for other arcjet systems show the potential for an order of magnitude increase in available thrust and double the available specific impulse [5]. Extrapolating the values for the demonstrated resistojets results in an arcjet estimated to have from 100 – 200 m/s of Δv and 5 – 170 mN of thrust for a 10kg satellite. This ΔV capacity would enable station keeping for a year between altitudes of 400 and 375 km at a solar maximum and ballistic coefficient of 50 kg/m^2 [7]. It also provides a commanded rapid deorbit capability out to 800km [7]. Thermal management for arcjets, similar to resistojets, is important in the development of the propulsion system. High temperature materials such as tungsten and tungsten alloys are chosen for the cathode and anode. Disposal of most spacecraft occurs as burnup during reentry. Arcjets with dense, high materials could be of concern to safety during reentry. Consideration needs to be given to using reentry as a disposal technique for such systems.

Propellants

A great deal of thought is devoted to choosing a propellant when designing a propulsion system. In general, the best propellants are those with a low molecular mass. A low molecular mass in exhaust products results in high exhaust velocities. Since higher heat capacities are associated with low molecular mass, more energy is imparted into the lighter molecules at a given temperature. This translates into being able to increase the propellant enthalpy and therefore its exhaust velocity. As shown earlier, high exhaust

velocities increase the system's thrust and specific impulse. The table below demonstrates the trend for increasing specific impulse with decreasing molecular mass for a set of gas propellants. Specific impulse is calculated for a 50 to 1 expansion ratio in vacuum.

Table 2 Gas Properties at 34.5 MPa and 293 K [5]

Propellant	Molecular Mass	Density (kg/m^3)	Ideal I_{sp} (sec)
Hydrogen (H_2)	2	28.4	284
Helium (He)	4	56.7	179
Methane (CH_4)	16	226	114
Nitrogen (N_2)	28	396	76

It is important to notice that though the specific impulse increases with decreasing molecular mass, the density also decreases with molecular mass. Low density propellants such as hydrogen require large propellant tanks. This is a difficult tradeoff for CubeSats that normally run out of available space before running out of a mass budget.

Chemical systems rely heavily on combustion products and temperature, for a given set of reactants, to determine system performance. Most chemical propellants are either toxic, hazardous or both. Increased hardware is then required to ensure a leak does not occur during assembly. Hydrazine is a common chemical propellant, but if spilled it is considered a catastrophic event. Current research is under way to find propellants that are less dangerous.

Cold gas and electrothermal systems have a more lenient selection when choosing propellants. Propellants are often inert and can be stored as a liquid reducing the needed

tank volume. Cold gas systems often chose propellants with a high vapor pressure. High vapor pressures allow the propellant to be stored as a liquid, a high-density storage option. As small amounts of heat are applied the propellant expands, self-pressurizing the tank and eliminating the need for other positive expulsion mechanisms. Electrothermal systems must consider any adverse effect from heating the chosen propellant. Propellants that 'coke', or leave residue when heated, can eventually clog the propellant feed system. Commonly used propellants in electrothermal systems are water, ammonia, and hydrazine. Other propellants being utilized that are not as common include sulfur dioxide and commonly available refrigerants such as R-134a and R-236fa. The table below lists the standard density for ammonia, water, and hydrazine.

Table 3 Density and Phase state for Electrothermal Propellants

Propellant	Density (kg/m^3)	Phase
Ammonia (NH_3)	0.7073	Gas
Water (H_2O)	998	Liquid
Hydrazine (N_2H_4)	1007	Liquid

Ammonia needs to be pressurized for storage as a liquid. Water has a higher density than ammonia and can be stored as a liquid at room temperature and pressure. Although water is less dense than hydrazine, it is only slightly less dense, and it is not as dangerous. Both ammonia and hydrazine are toxic to humans. Comparatively though, hydrazine is fatal in concentrations at an order of magnitude lower than those for ammonia [8], [9]. Water is an ideal choice for secondary payloads that adhere to a "do no harm" policy. Unfortunately, water use also introduces different potential problems. The water

temperature needs to be thermally moderated to prevent freezing. Contamination of the arcjet cathode. A combination of dimethyl ether and water-based propellant has been investigated. Erosion of the cathode increased when the mass percentage of water increased past 20 percent [10]. Other propellant combinations investigated included water and nitrogen as well as water and aluminum [11], [12]. Water has been successfully used but required a shielding gas to mitigate erosion of the cathode [13].

Space Power

Electrical power systems include a CubeSat's power generation, storage, and distribution to perform the mission. CubeSat power generation is accomplished almost exclusively with solar arrays. Storage is performed by either primary or secondary batteries. Power management and distribution (PMAD) is built to suit the specific needs of the satellite. As mission requirements change, so do required capabilities and power requirements.

Due to their reliability and technical maturity, solar cells are commonly used for power generation on nanosatellites. They are best suited for missions that last months to years, with power requirements below 20 kilowatts. Solar cells work better for earth orbital missions than for deep space missions. Power available to be captured using solar cells decreases further from the sun. Power generation is affected by the type of panels, the array area, eclipse period, and solar incidence angle. Cell efficiencies available to CubeSats can be as high as 28 - 32 percent [6]. The surface area of a CubeSat is small and not always positioned in a way that would allow a solar cell to generate power. Deployable solar panels are used to increase the available surface area. Solar array drive

assemblies have been developed to reduce incidence angle losses and increase average power generation.

Batteries for electrical storage are subcategorized as either primary or secondary batteries. Primary batteries serve as a single use where the chemical process is not reversible. Primary batteries have a higher energy density than secondary batteries. Secondary batteries are rechargeable but have a lower energy density. A trade-off becomes apparent between selecting enough primary batteries for the mission life or using low density rechargeable batteries. The table below shows the range of specific energy and energy densities for primary and secondary batteries.

Table 4 Primary and Secondary Battery Characteristics

Battery Type	Specific Energy (W-hr/kg)	Energy Density (W-hr/L)
Primary	100 - 340	330 – 1050
Secondary	35 – 200	60 – 230

The electrical power systems are directly impacted by the capabilities and operation of a given propulsion system. Cold gas systems often require less than 2 Watts of power to operate. Resistojets require between 10 and 55 Watts for operation. Miniaturized arcjets have been designed to operate with as little as 500 Watts, with more common low power systems requiring between 1 and 2 kW of power. Each of these different power requirements requires a different capability and can be fulfilled in a variety of methods. Electrothermal systems generally require large battery capacities and solar arrays to meet their power demands. Payload power available to nanosatellites typically range from 0.2 to 120 Watts [3].

Overview of Arcjet Systems

Arcjet thrusters were initially studied in the 1950's. Chemical systems favor impulsive orbital maneuvers due to their high available thrust but low specific impulse. Low specific impulse systems require more propellant to achieve the desired result. Increased propellant use increases system mass, resulting in even more propellant required to perform the transfer. A propulsion system with low thrust but high specific impulse normally increases the travel time, but decreases the required propellant. Arcjets were developed with specific impulses from 1000 to 2000 seconds with power requirements ranging from 1 to 200 kilowatts.

In the 1980's NASA began focusing on smaller, low power arcjets for north-south station keeping for use on communication satellites. Interest over the past two decades has now focused on arcjet systems for low earth orbit station keeping or formation flying. Current research has focused on arcjet systems that operate on sub-kilowatt power systems. Thrusters have been developed that operate even as low as 10 Watts. Smaller lower power arcjets are being developed to operate with less than 6 Watts of power and specific impulses less than 100 seconds. These systems are of less interest due to a resistojet's ability to produce similar specific impulse at similar or lower power requirements. Arcjets have been categorized into four different power classes; their characteristics are shown in the table below.

Table 5 Arcjet Characteristics [13]

Power Range	Thrust (mN)	Power (kW)	Specific Impulse (s)	Thrust efficiency (%)
Very Low Power	1-50	0.02-0.03	250-850	25-40
Low Power	80-300	0.5-2	420-1,000	30-40

Medium Power	400-1,200	5-15	600-1,300	35-50
High Power	1,500-7,000	30-200	800-2,200	25-50

Basic arcjet design involves running the working fluid through an electric discharge between two separated electrodes. The nozzle functions as the anode and is located downstream from the cathode. This polarity is important since the anode must sustain a high heat loading. Making the nozzle large and setting it as the anode enables it to sustain the high heat loading. Anodes and cathodes are usually made from tungsten or a tungsten-based alloys. Tungsten has a high melting point and is commonly used in similar welding processes. Propellant is injected upstream, flows past the cathode, through the constrictor, and expands into the supersonic portion of the nozzle. Injecting the propellant tangentially to the flow path generates a vortex that stabilizes the arc discharge and reduces erosion of the anode [14]. Three separate energy transfer modes for arcjet devices have been developed, as shown in Figure 4.

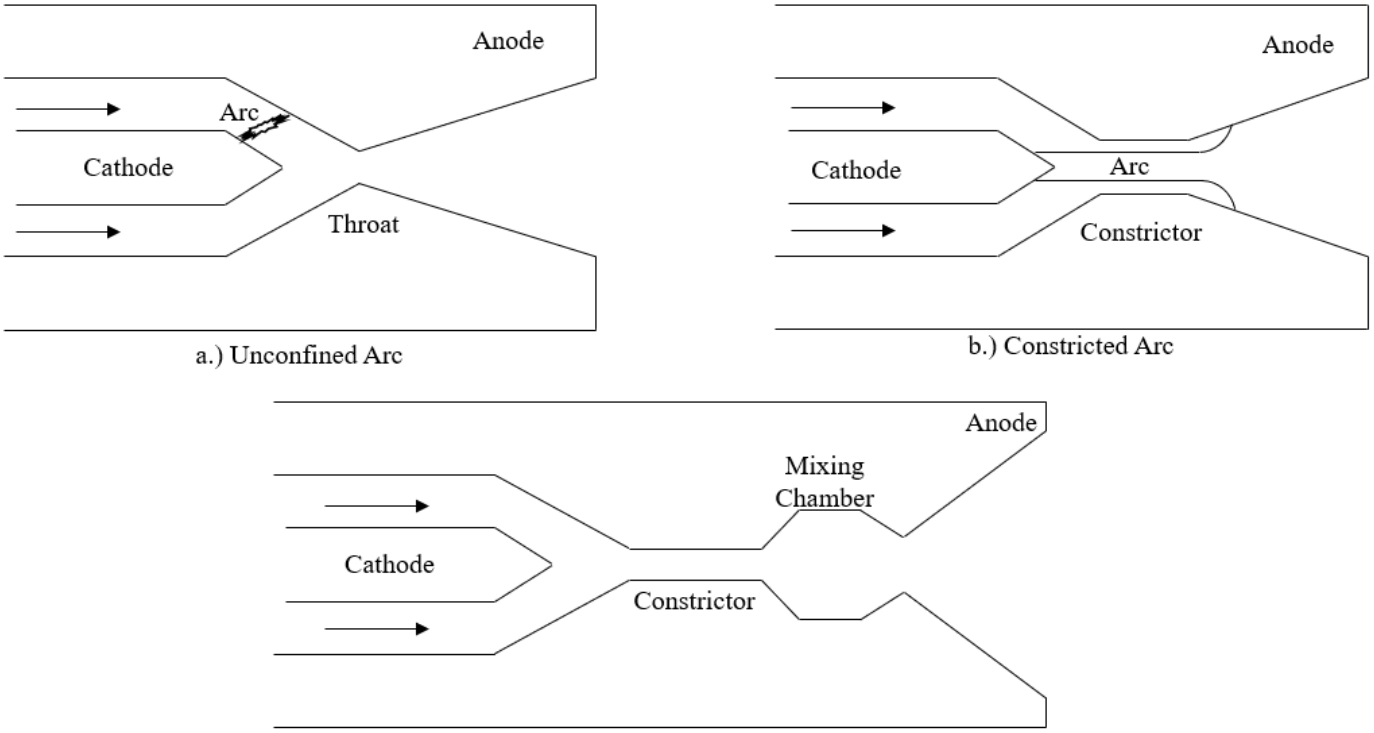

Figure 4 Arc Configurations

The first is an unconfined arc, also known as the low voltage mode, where the arc transfers from the cathode to the subsonic portion of the nozzle. This mode is expected to occur during low mass flows or quiescent flow conditions in the chamber. Second is a confined or constricted arc where arc attachment to the nozzle occurs in the supersonic portion of the nozzle. The arc is blown or forced through the constrictor to the supersonic portion of the nozzle. In the constricted arc a cold sheath of gas surrounds the high temperature, and low-density gas flow through the arc. Some configurations combine the constricted arc with a mixing chamber. The mixing chamber provides a more uniform heat distribution in the flow as well as a location for radicals to recombine. It can be a useful configuration when contamination from the arcjet exhaust is of concern. System performance of the third arc configuration, that features a mixing chamber, is worse than

for a constricted arc, resulting in a lower specific [15]. Nozzle expansion of the nozzle plays an important role in the design of the arcjet. Overexpanding the nozzle can push the arc back out of the supersonic portion of the nozzle. Larger ratios of exit area after nozzle expansion to constrictor area increases a system's specific impulse. A half-angle expansion of 15 degrees is the maximum angle for maintaining a stable arc in the nozzle. In smaller systems, below 1 kilowatt, viscous losses grow substantially due to the growing boundary layer. Smaller systems improve performance by maintaining a 15-degree half-angle expansion until the nozzle-throat area ratio reaches 50. At this point a more aggressive expansion at 45 degrees is used until the final nozzle-throat area ratio is reached [16]. Boundary layer viscous losses in the diverging nozzle are part of the reason small arcjet systems typically have lower exit velocities when compared to higher arcjet systems. Arc initiation occurs with a short high-voltage/ -low amperage pulse. Once the arc has transferred to the converging portion of the nozzle the voltage falls. As discussed earlier this is often referred to as an unconfined arc or the low voltage mode. When the arc is transferred to the diverging portion of the nozzle the voltage rises and is in the high voltage mode.

Arc ignition impacts design, erosion, and operation of arcjet devices. Early approaches used a process similar to the scratch start technique used in Tungsten Inert Gas (TIG) welding operations. In this method the cathode and anode are brought into contact, then propellant flow and current are applied. The cathode is then separated from the anode, establishing the arc. This method greatly reduces the complexity of the accompanying power processing unit. Most designs utilize a high voltage, 3 to 4 thousand volts, to initiate a Paschen breakdown. Erosion of the anode occurs after this

breakdown when the arc transfers to the converging portion of the nozzle. NASA's investigation of a miniaturized arcjet recorded shorting and cathode deformation as the cause of erosion [17]. Reducing current flow in the low voltage mode and increasing the mass flow rate minimizes erosion and pushes the arc through into the diverging section of the nozzle. Once in the diverging portion, current flow can be increased to the desired level for operation. Reliable arc initiation is one of the driving factors of concern when using arcjets for space missions. Additive manufacturing makes the development of new arcjet devices promising. Regenerative cooling passages can be easily integrated into the design to assist with thermal management. Different designs can be printed and investigated that assist with reliable arc initiation and attachment. Development of new designs and incorporation of green propellants may be able to make arcjets suitable for CubeSat propulsion.

Prior Work

Previous work at the Air Force Institute of Technology designed a compact CubeSat propulsion system [18]. The system envelope was designed to be less than 1U to allow for the power processing unit for a resistojet. An additively manufactured tank was printed from an aluminum alloy with an internal volume of 271 cm^3. The tank contains four mounting flanges allowing for different propulsion systems to be held through the center of the tank. An aluminum piston separates the internal space for propellant and hexafluoropropane, R-236fa. The refrigerant is heated by cartridge heaters that can be inserted into the tank. Heating the refrigerant provides the necessary pressure to feed the propellant into the propulsion device. Temperatures from 25°C to 55°C in the refrigerant

are expected to achieve pressures from 2.7 to 6.8 atmospheres. Each heater is monitored with a Type K thermocouple. Refrigerant pressure is monitored directly from a port in the tank lid. Microelectromechanical valves connect the tank to the propulsion system. Two pairs of parallel valves are connected in series to provide redundant controllable paths from the tank. Flow metering is accomplished by a restrictor placed in the flow path. This is expected to introduce transient shut down responses where propellant can still escape and boil off with little thrust produced, decreasing the system's specific impulse. Theoretical performance of the system is evaluated to range from 50 to 600 mN of thrust and 66 to 104 seconds of specific impulse [18]. This system can be easily modified for different CubeSat propulsion needs. Additional propellant can be added by extending the tank. Additional work is needed to refine the design and determine placement for the needed power processing unit.

Simplified Constricted Arcjet Analysis

Sanchez and Sakamoto's simplified analysis of arcjet thrusters is used to determine the initial design for the arcjet thruster. This analysis assumes that the arc has been forced through the constrictor and attached to the anode in the divergent portion. A two-stream approximation inside the constrictor separates the high temperature low density core flow from the outer flow. Gas flow is considered to flow in the outer cooler gas sheath. The arc resembles a plug through the flow. This analysis is a simple method for design without requiring numerical analysis. It is for this reason the simplified analysis is used for an initial design. The following sections outline the progression from a static arc to the arc in the parallel flow and to thrust and specific impulse calculations.

As the arc passes through the propellant flow heat is deposited into the gas through both ohmic heating and radial heat conduction. The heat from the center of the arc is transferred to the arc's periphery and then conducted radially to the buffer gas. This is modeled by the following equation (8) for the heating of the gas per unit length.

$$\frac{1}{2}\pi R_a^2 \sigma_c E^2 = 2\pi R_a \left(k\frac{\partial T}{\partial r}\right)_{r=R_a} \tag{8}$$

The gas electrical conductivity is given as a linear function of the temperature gradient in equation (9). This assumes that the electrical conductivity is zero outside of the arc radius, defined by the point at which the gas temperature is not high enough to exhibit electrical conductivity, noted as the edge temperature (T_e).

$$\sigma = \begin{cases} 0, & (T < T_e) \\ a(T - T_e), & (T \geq T_e) \end{cases} \tag{9}$$

Approximating the temperature gradient on the right-hand side of the equation as the difference between the arc centerline temperature (Tc) and the arc edge temperature.

$$\left(k\frac{\partial T}{\partial r}\right)_{r=R_a} \approx -2k_c\frac{T_c - T_e}{R_a} \tag{10}$$

The electrical conductivity, σ, varies radially through the arc; it is zero at the arc edge, R_a, and a maximum value at the arc's centerline. This analysis uses an approximation that the average electrical conductivity is half its centerline value, σ_c. The current can be calculated in two different manners shown in equation 11.

$$I = \pi R_a^2 E\frac{\sigma_c}{2} = \pi R_a^2 E \tag{11}$$

Substituting equation (10) into equation (8) and rearranging for the electric field which is then substituted into equation (11) yields a quadratic expression for the current (Eq. (12)).

$$I = \pi R_a\sqrt{2ak_c}(T_c - T_e) \tag{12}$$

A reference current and electric field produce non-dimensional units and figures.

$$I_{ref} = \pi R\sqrt{2ak_c}(T_e - T_w) \tag{13}$$

$$I^* = \frac{I}{I_{ref}} \tag{14}$$

$$E_{ref} = \frac{2}{R}\sqrt{\frac{2k_c}{a}} \tag{15}$$

$$E^* = \frac{E}{E_{ref}} \tag{16}$$

In parallel flow the arc energy balance now accounts for convection between the outer layer of the arc and the buffer gas represented in the following equation (Eq. (17)).

$$(\rho u)_{edge} 2\pi R_a \frac{dR_a}{dx} c_p\left(T_e - T_{buffer}\right) = 4\pi k_c (T_c - T_e) \tag{17}$$

Assuming inviscid flow, pressure, p, and dynamic pressure, ρu^2, are conserved along streamlines and are independent of the radial distance from the arc's center.

$$\rho u = \sqrt{\rho(\rho u^2)} = \sqrt{\frac{p(\rho u^2)}{R_{gas}T}} \tag{18}$$

$$\frac{(\rho u)_{edge}}{(\rho u)_{buffer}} = \sqrt{\frac{T_{buffer}}{T_{edge}}} \tag{19}$$

Most of the mass flow can be estimated to travel around the arc. Accounting for the growth of the arc along the constriction, the mass flow per area becomes

$$(\rho u)_{buffer} \approx \frac{\dot{m}}{\pi(R^2 - R_a^2)} \tag{20}$$

modeling the mass flow as an isentropic flow around the arc and assuming sonic flow at the nozzle throat. To produce a nondimensional mass flow, a reference mass flow is used, treating the entire constrictor as a converging nozzle.

$$\dot{m} = \left\{ \sqrt{\gamma} \left(\frac{2}{\gamma + 1} \right)^{\frac{\gamma+1}{2(\gamma-1)}} \right\} \frac{P_1 \pi \left(R^2 - R_{a,L}^2 \right)}{\sqrt{R_g T_0}} \tag{21}$$

$$\dot{m}_{ref} = \left\{ \sqrt{\gamma} \left(\frac{2}{\gamma + 1} \right)^{\frac{\gamma+1}{2(\gamma-1)}} \right\} \frac{P_1 \pi R^2}{\sqrt{R_g T_0}} \tag{22}$$

$$\dot{m}^* = 1 - r_{a,L}^2;\ r_a = \frac{R_a}{R} \tag{23}$$

A reference nondimensional length along the constrictor length is calculated as follows (Eqs. (24)-(25)).

$$x^* = \frac{x}{x_{ref}} = x \left[\frac{1}{2\pi} \frac{\dot{m} c_P}{k_c} \sqrt{\frac{T_{buffer}}{T_{edge}}} \right]^{-1} \tag{24}$$

$$x^* = \frac{1}{I^*} \left[\ln \left(\sqrt{\frac{1 + r_a}{1 - r_a}} \right) - r_a \right]_{r_{a0}}^{r_a} \tag{25}$$

The voltage drop across the constrictor can now be calculated as a function of the reference electric field, reference length, nondimensionalized current, and nondimensionalized arc radius.

$$V_{const} = E_{ref} x_{ref} \frac{1}{2I^*} \tag{26}$$

The voltage drop in the nozzle is a function of the attachment point length in the nozzle and nondimensionalized arc radius.

$$V_{nozzle} = 2 \sqrt{\frac{2k}{a}} \frac{1}{r_{a,L} \tan\theta} \ln \left(\frac{R_{N,att}}{R} \right) \tag{27}$$

The total voltage drop across the system is a combination of the voltage drop in the cathode, constrictor, nozzle, and anode. Power requirements for the system are then the sum of the arc current and voltage drop through the system.

$$V_{total} = V_{cathode} + V_{const} + V_{nozzle} + V_{anode} \tag{28}$$

$$P = IV_{total} \tag{29}$$

Assuming inviscid, compressible flow, a given expansion ratio, ϵ, provides a Mach number that is used to determine the exit pressure.

$$\epsilon = \frac{1}{M}\left[\frac{1 + \frac{\gamma - 1}{2}M^2}{1 + \frac{\gamma - 1}{2}}\right]^{\frac{\gamma+1}{2(\gamma-1)}} \tag{30}$$

$$P_e = \frac{P_o}{\left(1 + \frac{\gamma - 1}{2}M^2\right)^{\frac{\gamma}{\gamma-1}}} \tag{31}$$

The thrust and specific impulse are determined, assuming supersonic and isentropic flow conditions through a nozzle. Determining the thrust depends on the exit pressure and Mach number of the corresponding flow, Eq. 20.

$$F = P_e A_e (1 + \gamma M^2) \tag{32}$$

Specific impulse is directly proportional to the thrust produced and inversely proportional to the mass flow.

$$I_{sp} = \frac{F}{\dot{m} g_o} \tag{33}$$

This analysis assumes that the arc has been pushed through the constrictor and is not attached to the converging portion of the nozzle. This analysis provides a theoretical estimate of thrust, specific impulse, and power requirements for a given design.

III. Methodology

Chapter Overview

This chapter covers the arcjet propulsion design, and equipment for testing. Physical parameters for the arcjet were chosen for the initial build. Assembly of the tank is based off previous research with minor modifications. Changes to the tank were made to correct valve orientation and account for the arcjet interface. A vacuum chamber is used to test in a near vacuum environment. Pressure sensors monitor the vacuum chamber and tank pressures. The thrust stand developed from previous research utilizes a low-profile load cell to measure thrust performance. Output from the sensors is collected using two separate National Instrument (NI) Data Acquisition, DAQ, devices and displayed using LabVIEW's user interface.

Arcjet Design

Tank dimensions and power limitations serve as the foundation for initial design of the arcjet. Standard dimensions for CubeSats are given as multiples of Units or "U"s. A 1U size is a 10 centimeter cube, a volume of one liter. It was desired for the arcjet to fit in the internal cavity of the tank to maintain the 1U sizing of a final design. The internal length of the tank measures at 70 mm with a diameter of 48 millimeters. Achieving expansion ratios greater than 50 requires a constrictor diameter less than 6 millimeters. A constrictor diameter of 2 millimeters was chosen with a length of 10 millimeters. The exit of the constrictor was then expanded by a factor of 4 at a half angle of 15 degrees. This allows for easy visualization of arc behavior inside the constrictor. A propellant feed

interface using a 1/16” National Pipe Thread (NPT) tapped hole was added. A cross sectional view of the interior of the core is shown in Figure 5.

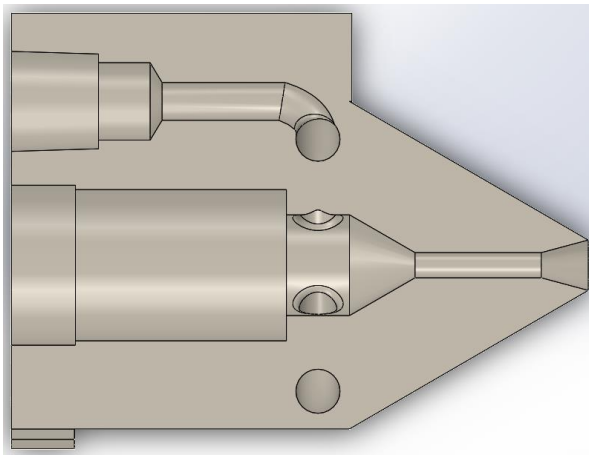

Figure 5 Arcjet Core Section View

Commonly available Tungsten rods range in size from 0.040 to ¼ inches. A 3/32-inch diameter rod was chosen to fit commonly available M4 ceramic washers, and M5 ceramic insulating sleeve washers were used to electrically insulate and center the tungsten cathode. Lanthanated and pure Tungsten rods were selected for use as the cathode. Lanthanated TIG electrodes contain between 1.3 and 1.7 percent lantha. Lanthanated rods are chosen for DC applications where the Tungsten rod will act as the cathode, also known as DC Electrode Negative, DCEN. Tungsten Lanthanum alloys demonstrate good arc initiation and stability [19]. Pure Tungsten electrodes were chosen as a baseline for comparison against the Lanthanated rods. A 5 mm set-screw collar was used to maintain the electrode gapping space. A custom retaining screw was made to hold the assembly in place. Figure 6 shows the setup of the tungsten cathode, ceramic washers, set screw collars, and retaining nut within the arcjet core. Insulation of the set screw collar was accomplished with a 3D-printed Polylactic Acid (PLA) sleeve.

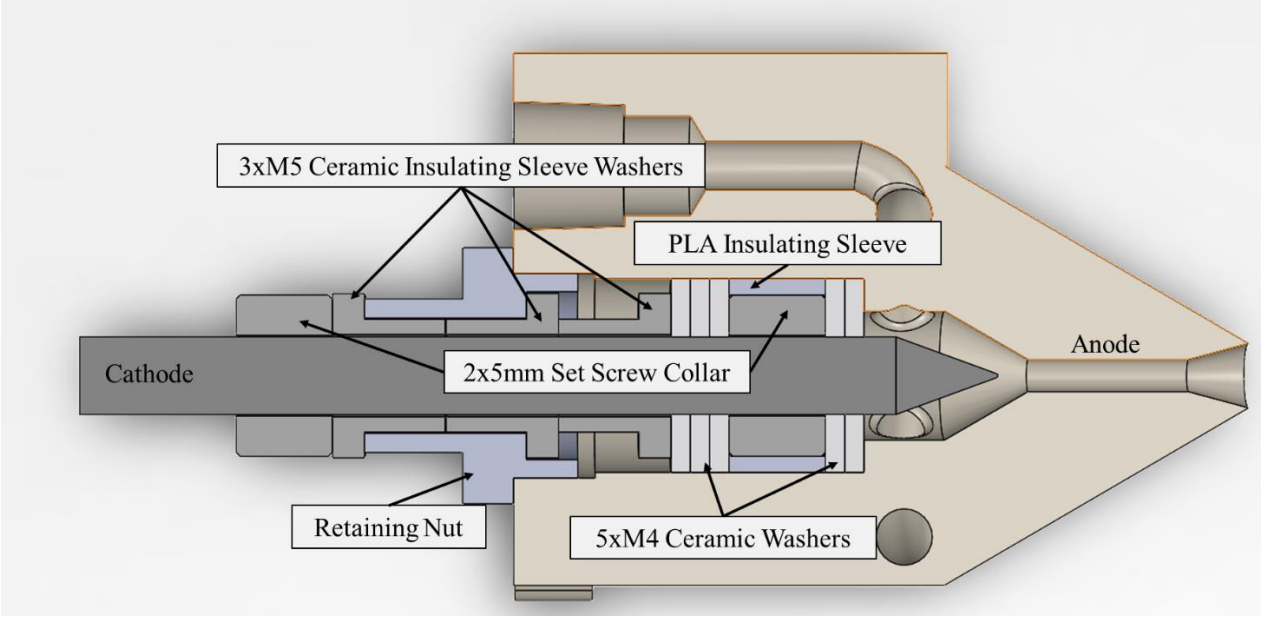

Figure 6 Arcjet Core and Cathode Assembly

Figure 6 shows that the anode also serves as the housing for the cathode and propellant feed system. The arcjet anode was additively manufactured using Inconel. Theoretical performance of the system is detailed in Chapter 4. Assembly of the tank and arcjet is described in the next section.

Assembly

Assembly of the tank and arcjet closely resembles the setup as described in the paper, “Design of a High Reliability Compact CubeSat Propulsion system” [18]. Previous construction of the tank systems resulted in a refinement of the system implemented in this work. It was discovered that the valves had a directionality that was not originally apparent. The tank was changed from the previous work to change the orientation of the valves. Other changes included using an external pressurized tank of carbon dioxide to provide a constant tank pressure during testing. Tank pressure is monitored using the 19mm series Honeywell pressure transducer, part number 19C200PV4K. Lee Company

IEP extended performance solenoid valves, model IEPA1211241H, controlled propellant flow into the arcjet. A Lee Company Jeva series, flow restrictor was placed inside a 1/16" NPT Swagelok™ fitting with custom internal machining that joins the tubing from the valve manifold to the propellant inlet of the arcjet. Figure 7 shows the assembled tank and arcjet system inside the vacuum chamber.

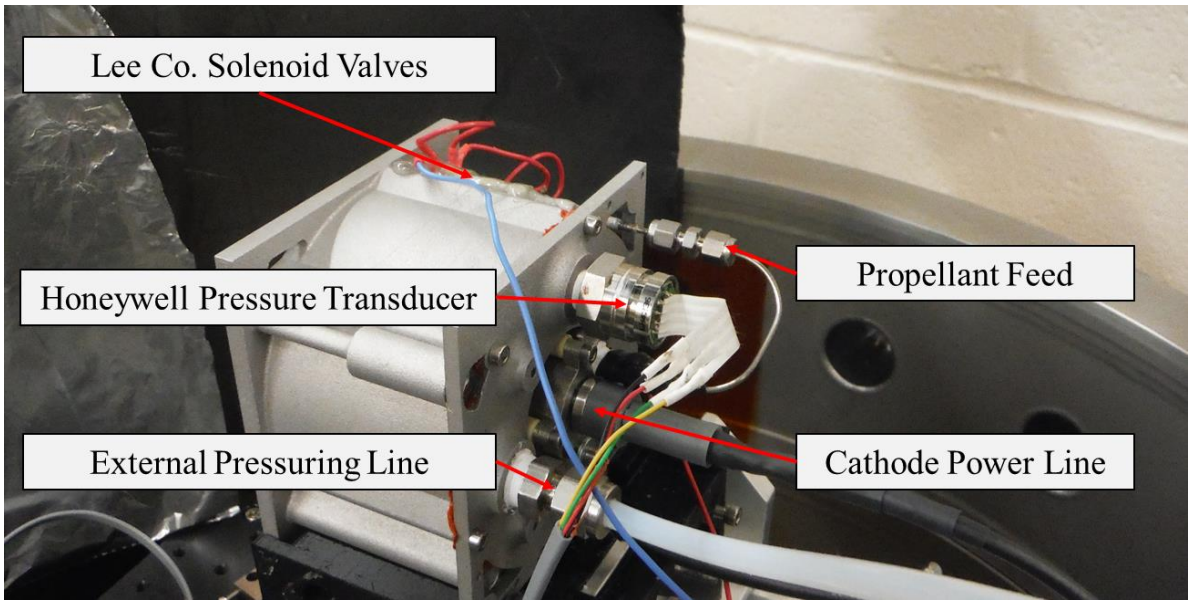

Figure 7 Assembled Tank and Arcjet

Assembly began by installing the four valves and soldering them together in series for connection to an external power supply. The valves were then connected to the propellant manifold and epoxied in place to prevent leaking. A 1/16" to 1/16" Swagelok™ connector was installed at the exit of the propellant manifold. The 1/16" tubing was bent to connect the manifold to the 1/16" NPT arcjet inlet. Coaxial cable was used to connect the cathode and anode to the micro-arc power supply.

Laboratory Facilities

Vacuum Chamber

A vacuum chamber was used to simulate the space environment for testing. A bell vacuum chamber equipped with a roughing pump and oil diffusion pump were used for this research.

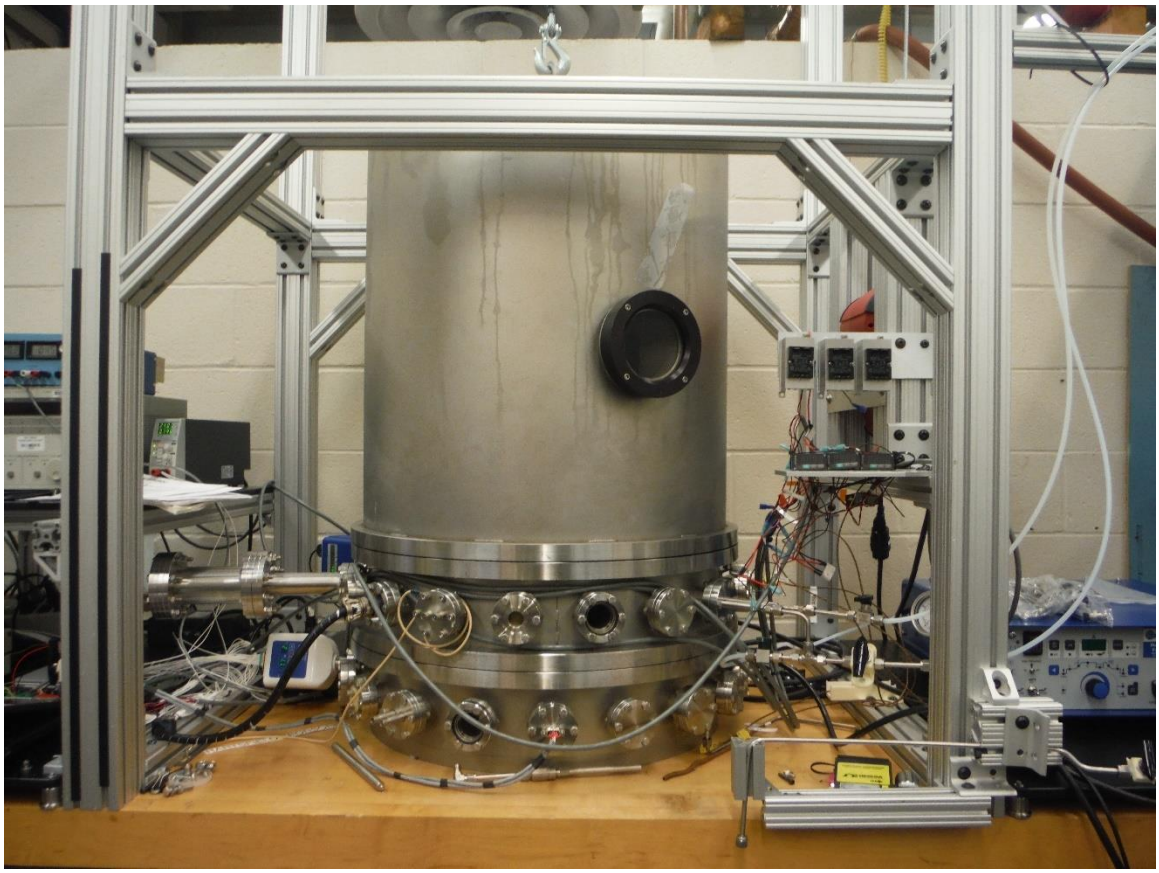

Figure 8 Vacuum Chamber in Operation

The chamber has 36 through ports that were used to place lines inside the vacuum chamber that provide fluid, power, and signal connections to the arcjet, tank valves, and sensors as well as ports for visual inspection of the system. The roughing pump was used to drop the pressure inside the tank below one Torr, and the oil diffusion pump can reduce the pressure to 10^{-7} Torr. The vacuum chamber is mounted on a table

with four air cushions that filter out external noise above 5 Hz. A Televac CC-10, a wide range active vacuum gauge, monitors pressure inside the tank. The Televac CC-10 is capable of measuring pressure from 10^{-9} Torr to atmospheric conditions. Torr is often used as the unit of pressure throughout the analysis in chapter 4 as a comparison against the output of the Televac CC-10.

Electrical Power System

The electrical power system for arcjets needs to be able to transform a satellite's bus power to a high voltage at low current for arc initiation. Once the arc has transferred the resistance drops and the electrical power system needs to prevent large currents from destroying the electrodes. Erosion of the anode can be reduced by reducing the arc striking amperage and then increasing the current to operational current levels [20]. A Pro-Fusion Dual Arc 82 HFP Micro-Arc power supply by Elderfield and Hall Inc. was chosen to simulate the arcjet power processing unit.

Figure 9 Pro-Fusion Power Supply

Arc initiation occurs with a high voltage pulse 6kV over 2 microseconds at 60 to 70 Hz [21]. This system was chosen for its ability to maintain an arc at amperages as low as 0.1 amps to 20 amps in 0.1 amp increments. Initiation current could be set as low as 5% of the main weld current with programmable time duration set for each point.

Thrust Stand

Thrust were completed using a double inverted pendulum thrust stand. A miniature platform load cell from strain measurment devices was mounted to the thrust stand. The S251 load cell from Strain Measurement Devices with a rated capacity of 0.2 kgs (approximately 2N) was selected for use. Using a Wheatstone bridge circuit, the load cell produces an electrical response due to the deflection of the thrust stand. Nine washers with an average mass of 13.3614g with a standard deviation of 0.0510g were used to generate the calibration curve and check the hysteresis. Appendix A details the input mass, corresponding force applied, and output from the load cell to generate the calibration curve. Expected arcjet thrust is expected to be between 0.1 and 1 Newtons. The calibration curve covers an applied force from 0 to 1.1 Vewtons. Figure 10 shows the generated calibration curve.

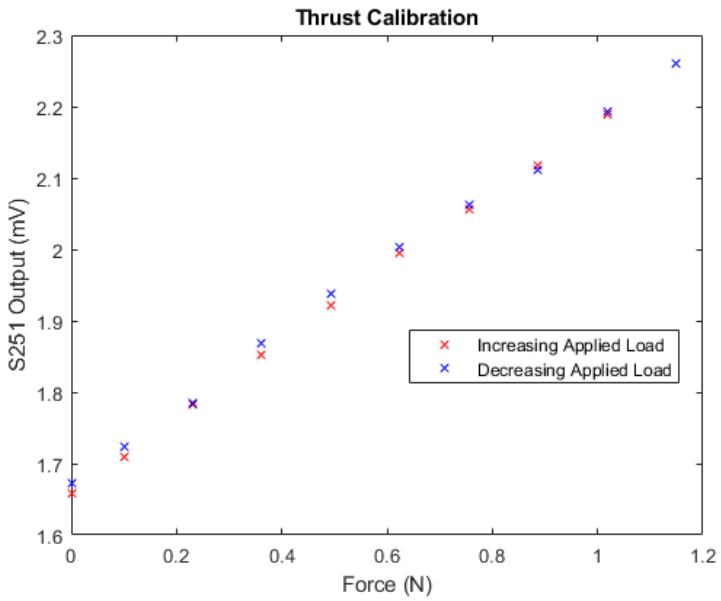

Figure 10 Thrust Calibration

The calculated coefficient of determination, R2, is 0.998 which is indicative of a good linear fit for the calibration cell. The maximum hysteresis of the system is 0.0171 and corresponds to a difference of 33 mN of measured thrust. The linear model is given in the following equation for the thrust measurements taken.

$$y = 0.5143 \frac{mV}{kg} x + 1.6688\ mV \tag{34}$$

Data Acquisition

Data acquisition is handled by two separate NI devices. Vacuum chamber pressure from the Televac CC-10 is connected to a multifunction I/O device, NI USB-6251, via a terminal block, NI SCB-68.

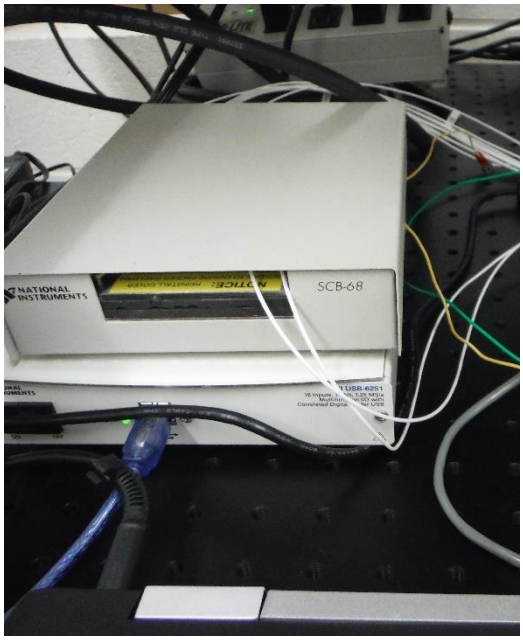

Figure 11 Multifunction I/O and Terminal Block

Tank pressure and load cell output are connected to a C series strain bridge input module, NI-9237, via a connection block, NI's CB-37F-LP.

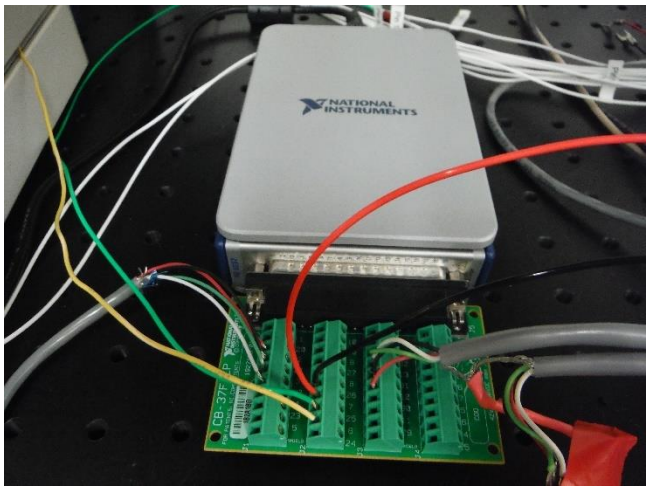

Figure 12 C Series strain bridge input module and connection block

Figure 13 shows the LabVIEW user interface for collection of pressure and thrust measurements.

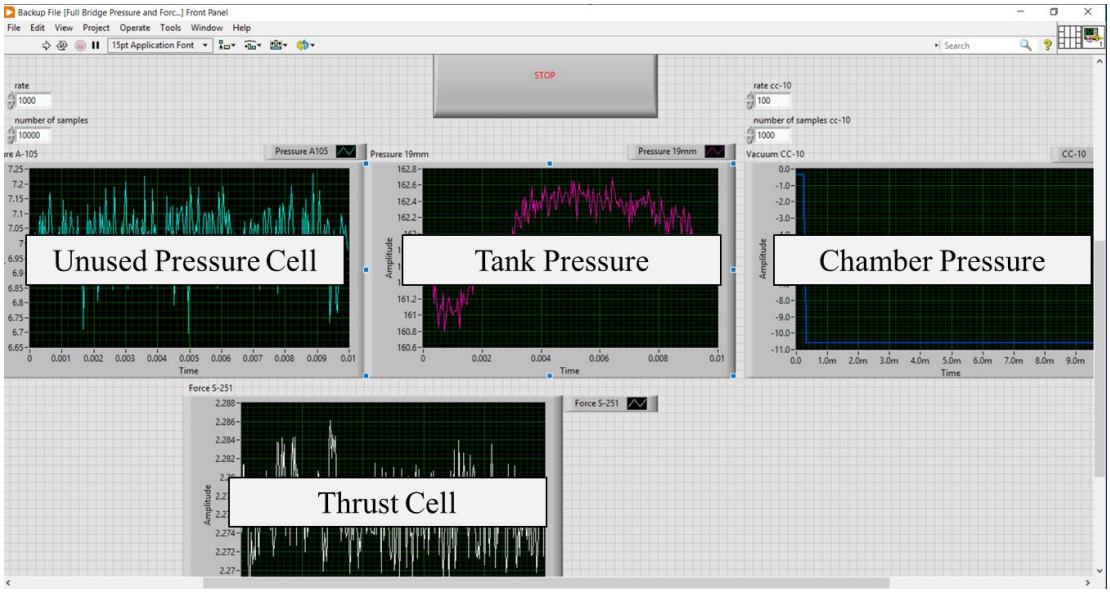

Figure 13 LabVIEW User Interface

The block diagram below shows the connection for the different sensors and data accumulation.

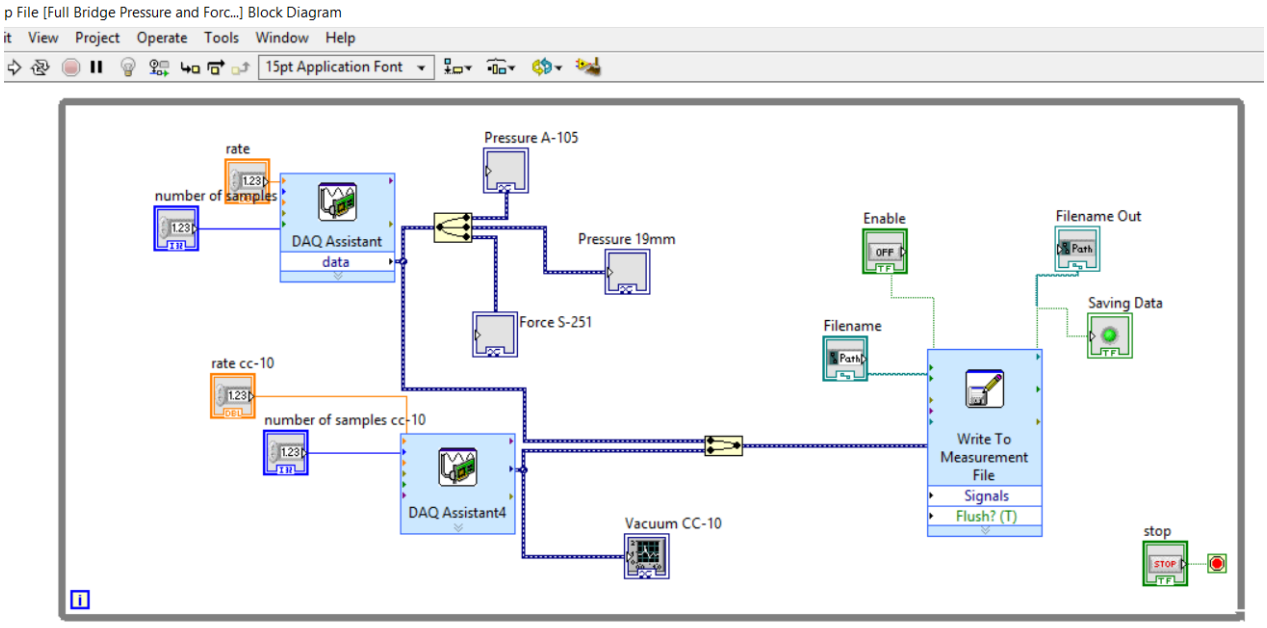

Figure 14 Sensor Block Diagram

Summary

This chapter covered the methodology used for experimental measurement of the designed arcjet system. Design of the arcjet follows previous designs of other larger arcjet systems. The arcjet anode was additively manufactured from Inconel and further machined to the design specifications. The vacuum chamber is capable of simulating pressures similar to a space environment. Sensors for pressure and thrust are routed through separate DAQ devices then displayed and recorded using NI's LabVIEW graphical programming environment.

IV. Analysis and Results

Chapter Overview

This chapter focuses on the analytical results of the tank design. Feasibility of the system is compared to other electrothermal propulsion elements. A rudimentary power processing unit and associated batteries design is performed to understand the potential space and mass requirements. Observations of the system during arc initiation are provided along with the measurements collected from the thrust stand's load cell.

Theoretical Design Performance

Martinez and Sakamoto's simplified analysis [22] as discussed in Chapter 2 begins with the arcjet physical parameters and working fluid properties. The goal of this research is to use H_2O as the working fluid. The temperature of the water is kept above freezing to prevent damage to the propellant tank [18]. A temperature of 20°C is assumed for both testing and operational use. It is also assumed that the water changes to steam when injected into the chamber of the arcjet. At 20°C the vapor pressure of saturated steam is 2.338 kPa [23] or 17.54 torr. Satellites in Low-Earth Orbit, LEO, are categorized at altitudes less than 3,000 km with most below 900 km [7]. Pressure between 100km and 900km range in magnitude from 10^{-2} to 10^{-8} Pa (10^{-4} Torr to 10^{-11} Torr). Given an input pressure from the refrigerant of 272 kPa at 25°C there would need to be a pressure drop in the lines from the tank to the chamber of arcjet of 268 kPa. Properties of water vapor are given below in Table 6 [23] along with estimated properties of electrical and thermal conductivity [24], [25].

Table 6 Steam Properties

Molar Mass, M (kg/kmole)	18.016
Specific Heat at Constant Pressure, c_p (kJ/kg-K)	1.867
Ratio of specific Heats, γ	1.33
Specific Gas Constant, R_g (kJ/kg-K)	0.461
Thermal Conductivity of Water Vapor, k (W/m/K)	0.0184
Gas Electrical Conductivity Est., a (Si/m/K)	0.08

The constrictor diameter is 2 millimeters with a length of 10 millimeters. Mass flow through the system is controlled by changing pressure in the propellant storage tank and is metered by a Lee JEVA series restrictor. A pressure difference between the tank and the arcjet chamber of 255 kPa results in a flow of 125 milligrams per second through the restrictor. Initially the arc edge temperature is estimated to be 5000 Kelvin. The arc current is set at 2 amps from the power supply. Stepping through the simplified analysis provides the following results.

$$I_{ref} = \pi(0.001\text{m})\sqrt{2\left(0.08\frac{\text{Si}}{\text{m K}}\right)\left(0.0184\frac{\text{W}}{\text{m K}}\right)}\,(5000\text{-}298\text{ K}) = 0.801\text{ A} \tag{35}$$

$$I^* = \frac{2\text{ A}}{0.801\text{ A}} = 2.495 \tag{36}$$

$$x_{ref} = \frac{\left(125 * 10^{-6}\frac{\text{kg}}{\text{s}}\right)\left(1867\frac{\text{J}}{\text{kg K}}\right)}{2\pi\left(0.0184\frac{\text{W}}{\text{m K}}\right)}\sqrt{\frac{333\text{ K}}{5000\text{ K}}} = 0.197\text{ m} \tag{37}$$

The non-dimensional value of x at the end of the constrictor is denoted as x^*_L. and is calculated using equation 24 from Chapter 2.

$$x_L^* = \frac{0.01\ \text{m}}{0.208\ \text{m}} = 0.051 \tag{38}$$

Setting this result as the value for x^* from equation 25 and solving for r_a gives a result for r_a of 0.644. Plugging this value of r_a into equation 23 gives the following results.

$$\dot{m}^* = 0.575 \tag{39}$$

$$\dot{m}_{ref} = \frac{\dot{m}}{\dot{m}^*} = 8.69 * 10^{-5}\,\frac{\text{kg}}{\text{s}} \tag{40}$$

Using this value for in equation and solving for P_1 in equation 22 provides the following result for chamber pressure.

$$P_1 = 15{,}255\ \text{Pa} \tag{41}$$

At 25°C the vapor pressure of water is 3,169 Pa [23]. This would result in liquid water entering the chamber. The temperature of the water would need to be 55°C at this pressure to result in saturated water. Iterating with gas temperature results in a chamber pressure equal to 15,751 Pa. At 55°C this pressure coincides with saturated water. A small transient time is expected where water would flow into the chamber until the temperature had risen and steam entered the chamber. Given the expansion ratio of 4, the Mach number at the exit of the nozzle is calculated using equation (30) leading to the exit pressure, thrust and specific impulse given an exit area of $1.26*10^{-5}$ m^2.

$$M = 2.82 \tag{42}$$

$$P_e = 534\ Pa \tag{43}$$

$$T = 0.078\ N \tag{44}$$

$$I_{sp} = 159\ s \tag{45}$$

Power requirements for this system are calculated using the reference electric field from equation 15 and to determine the voltage drop in the constrictor and the nozzle. The maximum voltage drop across the nozzle would be at the end of the nozzle.

$$V_{const} = 30\ V \tag{46}$$

$$V_{nozzle} = 5.41\ V \tag{47}$$

It is assumed that the voltage drop across the cathode and anode will be similar but not greater than 20 V [26].

$$V_{total} = 75.41\ V \tag{48}$$

Estimated power for the system is calculated as 151 Watts for steady-state operation. One of the assumptions made is the temperature of the arc at the edge. TIG arcs range in temperature from 5,000 to 12,000 Kelvin. Varying the assumed arc temperature changes the estimated thrust and specific impulse as shown below in Figure 15.

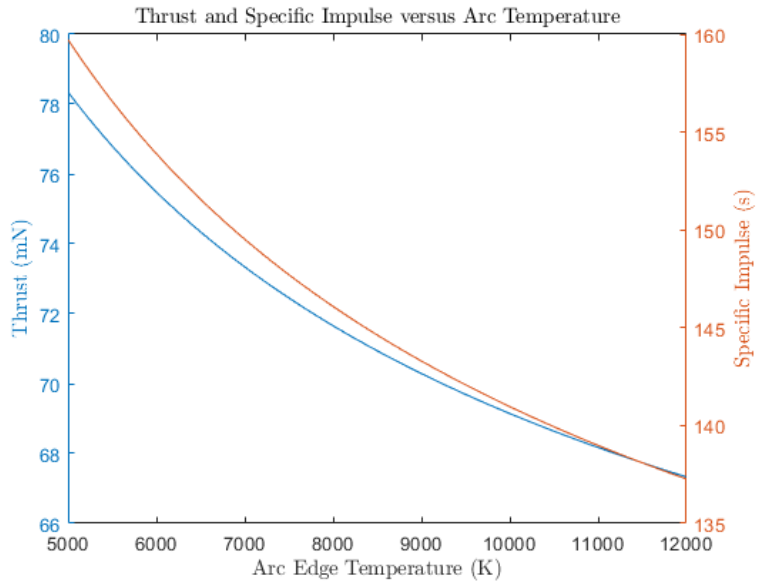

Figure 15 Thrust and Specific Impulse as a Function of Arc Edge Temperature

Varying the arc edge temperature does vary the estimated thrust and specific impulse of the system. However, the simplified analysis is useful as a simple method of obtaining an

order of magnitude estimate for the performance of the arcjet systems. Varying the mass flow has a much larger impact on propulsion performance.

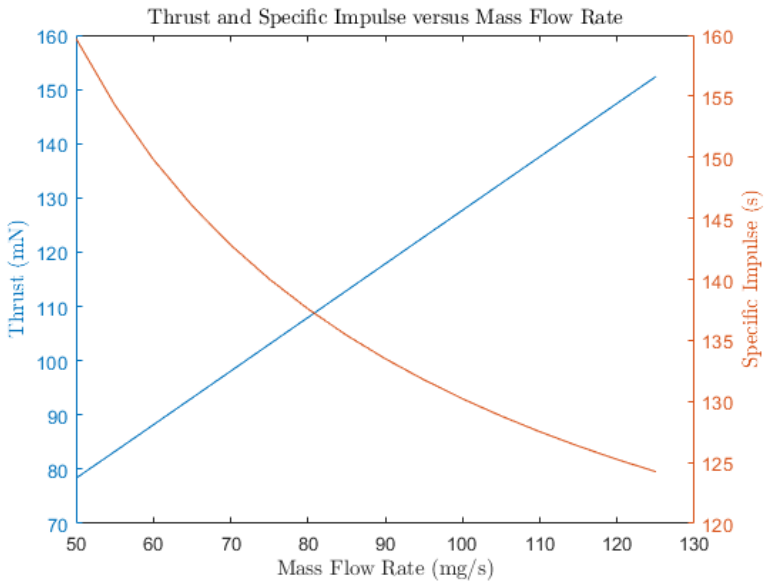

Figure 16 Thrust and Specific Impulse as a Function of Mass Flow

This analysis provides the bounds for expected performance of the system. Thrust for the system ranges from 70 to 150 milliNewtons and 125 to 160 seconds of specific impulse.

Electrical Power System Design

Estimated power requirements from the simplified analysis range from 145 to 165 Watts. State-of-the-art nanosatellites have payload power requirements below 120 Watts with most microsatellites having payload power below 180 Watts. Given the tank's capacity of 246 grams of water [18] and a maximum mass flow of 125 milligrams per second the batteries will only be needed for slightly over a half hour. If the minimum mass flow is set at 10 milligrams per second, the system is expected operate for almost 7 hours. Battery capacity, in Watt hours, is determined using the following equation [7].

$$\mathrm{C} = \frac{PT}{\mathrm{DoD\ N\ n}} \tag{49}$$

In the above equation *P* is the power required during operation, *T* is the time, in hours, during operation, *DoD* is the depth of discharge, *N* is the number of batteries, and *n* is the efficiency of battery-to-load transmission. The power load is 200 Watts, providing a margin of safety for inefficiencies. The maximum time expected time for a single burn is 30 minutes that corresponds to the maximum mass flow and emptying the tank. Lithium-ion batteries are commonly used in state-of-the-art nanosatellites and microsatellites [3], [6] where the depth of discharge is normally limited to 20% [7]. A limited depth of discharge allows the batteries to last for thousands of hours. It is imagined in this case that the system only need to work for tens of cycles. In this scenario the depth of discharge is taken to 100%. A 90% battery-to-load transmission efficiency assumed. This results in a battery capacity of 111 Watt-hours. Redundancy is recommended and two batteries are chosen with a total capacity of 222 Watt-hours. Lithium-ion batteries have specific energies as high as 260 Watt-hours per kilogram and as low as 112 Watt-hours per kilogram [3]. Using the more conservative value of 112 Watt-hours per kilogram results in a battery pack with a mass of 2 kilograms. Previously designed power processing units for miniaturized arcjets resulted in systems with a mass of 0.45 kilograms that operated at power levels between 150 and 350 Watts [27]. The estimated final mass for the required electrical power subsystem is 2.45 kilograms. The dry tank and arcjet mass measured at 844 grams. Adding the dry tank mass to the estimated power mass, above results in a mass of 3.29 kilograms and a specific power for the arcjet powerplant, α, as 46 Watts per kilogram.

Energy densities for Lithium-ion batteries range from 200 – 400 Watt-hours per liter [6], [7]. The estimated required volume for the above system ranges from a little over 0.5 liters to a little over 1 liter (0.5U to 1U). Summing the tank volume of 1U with the estimated battery volume results in a system that occupies a space between 1.5U and 2U. A 6U CubeSat might be able to accommodate the system. For 3U CubeSats this system would take up half or more of the available space.

System Comparison

Flight performance for electrothermal systems can be viewed as a function of power, time, specific impulse, propellant, payload and powerplant masses [5]. Payload mass fractions can be modeled as a function of the propellant burn time t_p, propellant exit velocity u_e, specific power α, ΔV required, and efficiency η as shown in equation (50) [5].

$$\frac{m_o}{m_{pl}} = \frac{e^{\frac{\Delta V}{u_e}}}{1 - \frac{\left(e^{\frac{\Delta V}{u_e}} - 1\right) v^2}{(2\alpha t_b \eta_t)}} \tag{50}$$

The inverse of the above equation is the payload mass fraction. The payload mass fraction is a satellite's mass excluding the propellant and powerplant system. It should be noted that it does not exclude the power source or its conversion system [5]. Propellant exit velocity is obtained by rearranging equation 3 as a product of specific impulse and the gravitational constant. Given the maximum mass of nanosatellites of 10 kilograms and the propellant capacity of the tank of 246 grams, the propellant mass fraction is 0.0246. Thruster efficiency is a ratio of jet power produced to electrical power input [5].

$$\eta_t = \frac{\frac{1}{2}\dot{m}v^2}{IV} \tag{51}$$

The following plots show the relationship for attainable ΔVs given the propellant mass fraction over a range of specific impulses, time, and the corresponding payload mass fraction.

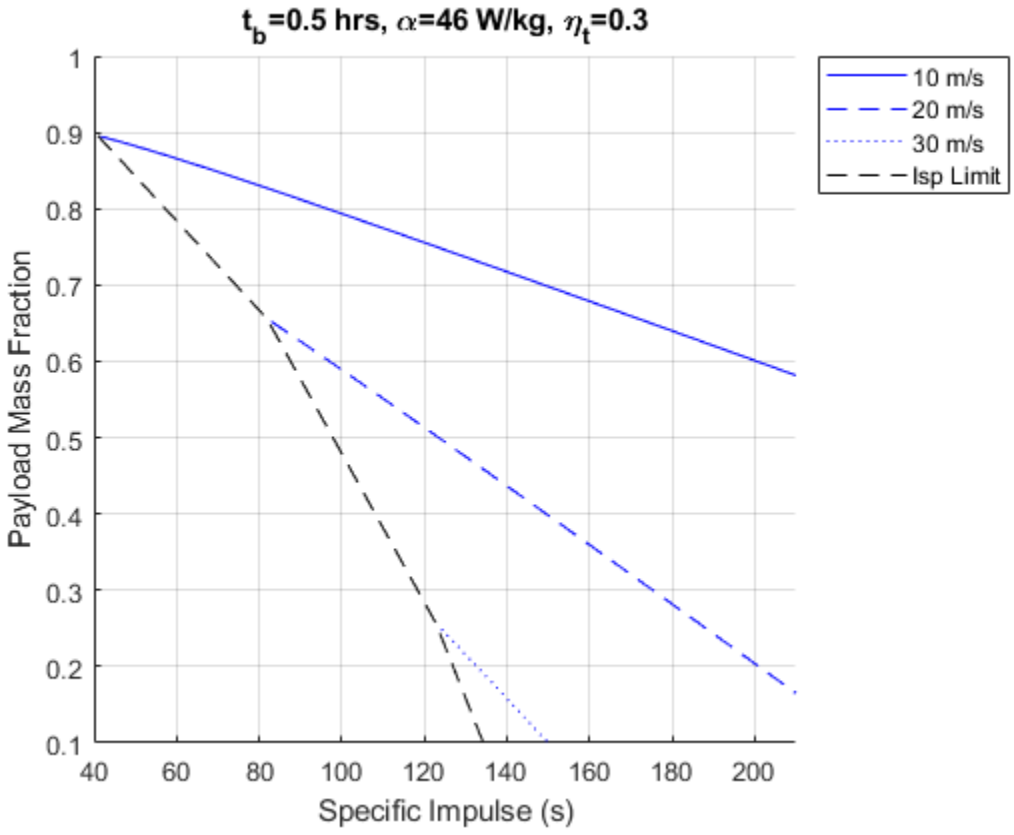

Figure 17 Arcjet Payload Mass Fraction vs Specific Impulse - ½ hr

The dashed black line, Isp limit, bounds the graph where systems with specific impulses less than the values to the left of this line would not be able to achieve the given ΔV. To achieve higher ΔV the payload mass fraction decreases. Increasing the propellant mass fraction would shift the specific impulse down and to the left achieving higher ΔVs at lower payload mass fractions. Decreasing the propellant mass fraction results in this line shifting up and to the right with lower ΔVs achieved. Increasing the specific impulse

requires a larger powerplant mass fraction. Increasing the propellant burn time results in increased available mass fractions for a given ΔV and specific impulse as shown in Figures 18-19.

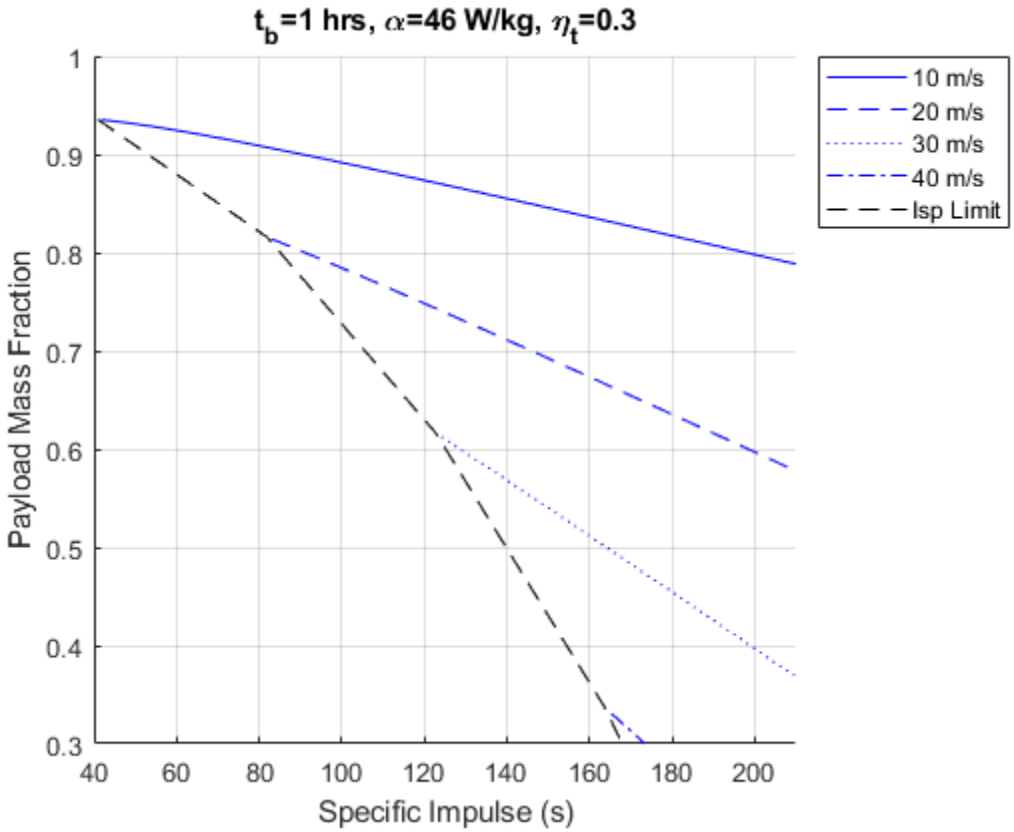

Figure 18 Arcjet Payload Mass Fraction vs. Specific Impulse - 1 hr

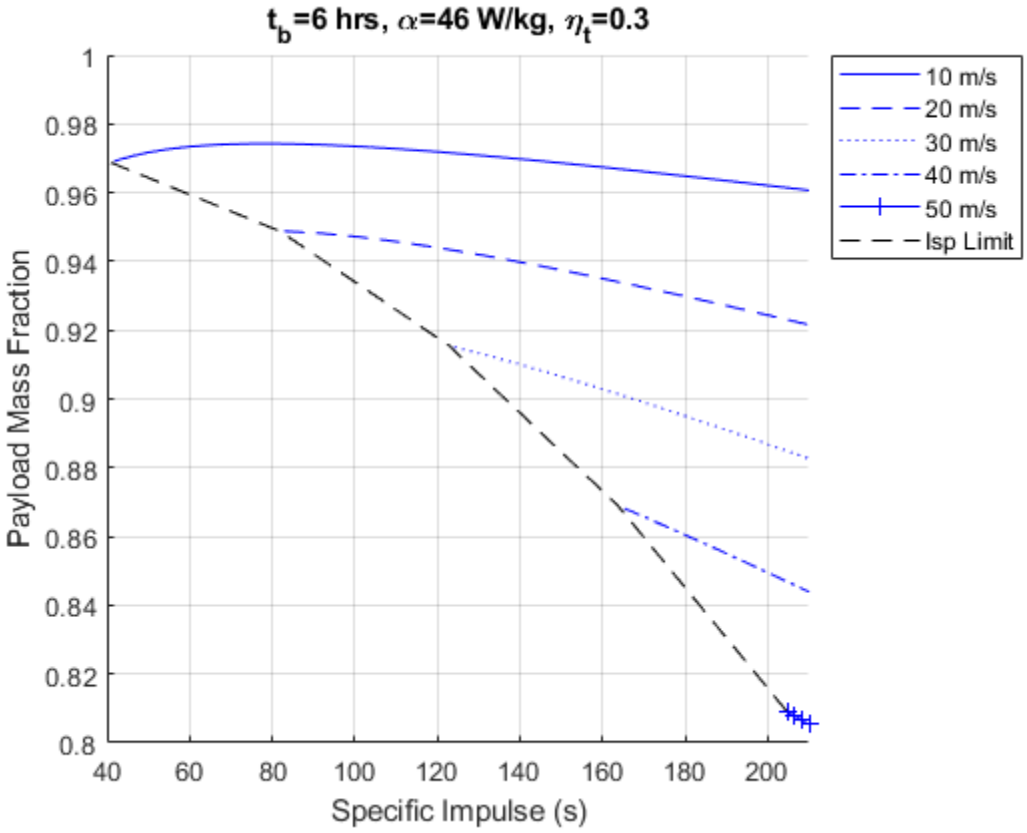

Figure 19 Arcjet Payload Mass Fraction vs. Specific Impulse - 6 hrs

The burn time in Figure 18 corresponds to a mass flow of 50 mg/s and Figure 19 to a mass flow of 10 mg/s. The payload mass fractions in these charts increase to percentages more realistic to what can be supported in CubeSats. The payload mass fraction only excludes the propellant and power plant masses. There are roughly another three tenths of mass fraction that are dedicated to structural mass [7]. At low mass flows and longer burn times the system can achieve higher ΔVs. Resistojet systems have demonstrated slightly lower specific impulse values [13], similar or greater specific power, but much higher thruster efficiencies [5] between 0.8 and 0.9. Plotting the payload mass fraction with an efficiency of 0.9 and a specific mass of 100 Watts per kilogram is shown in the following figures.

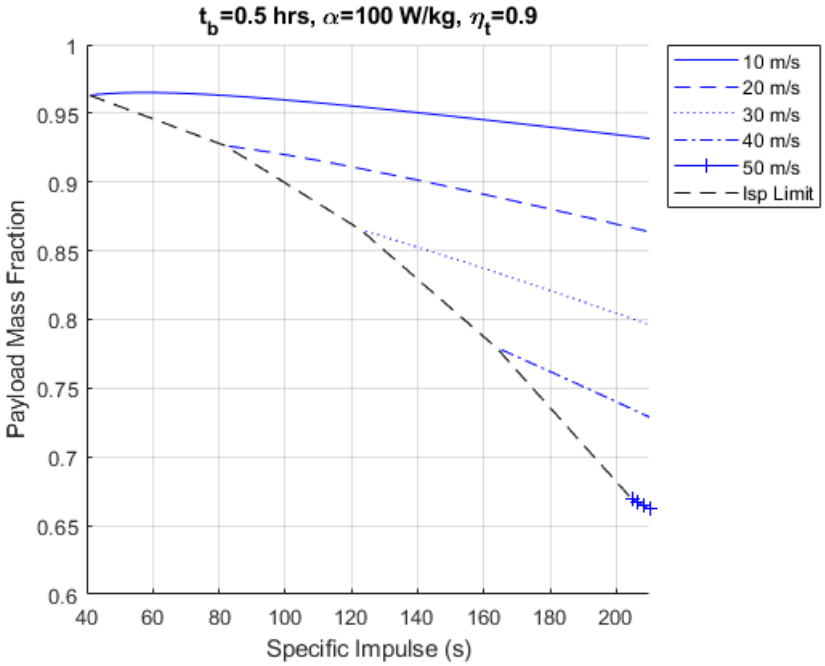

Figure 20 Resistojet Payload Mass Fraction - ½ hr

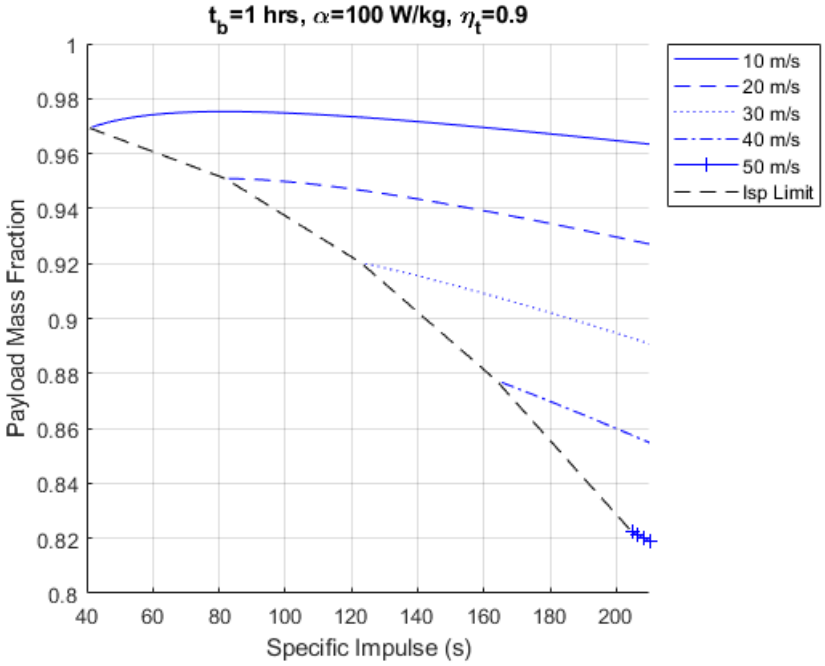

Figure 21 Resistojet Payload Mass Fraction - 1 hr

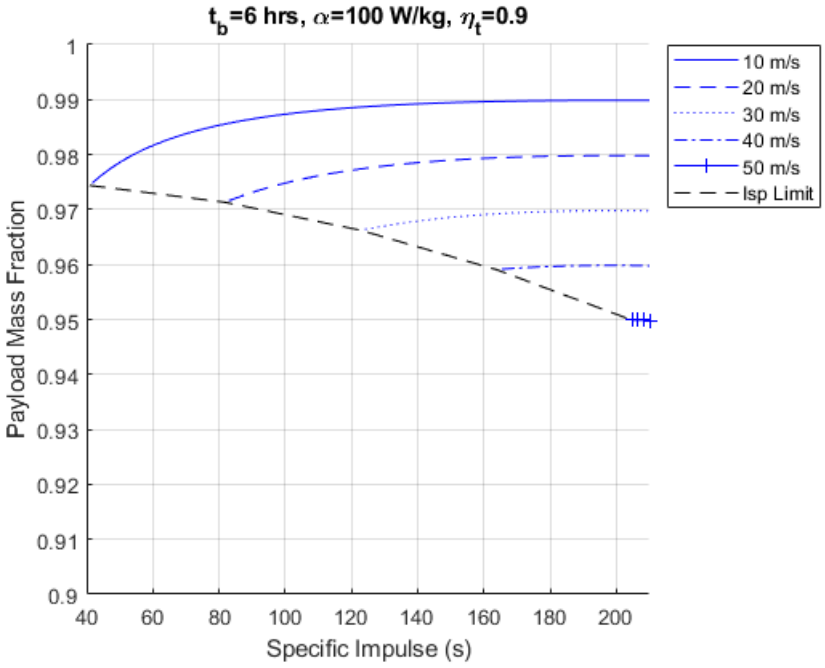

Figure 22 Resistojet Payload Mass Fraction - 6 hrs

Higher efficiencies results in a higher available payload mass fractions for a given specific impulse. The arcjet is expected to achieve greater ΔVs at payload mass fractions less than 0.9 for a given transfer time. A representative resistojet is expected to achieve mass fractions that are practical for use in CubeSats but may not be able to meet ΔV values greater than 30 m/s. In summary arcjet systems provide higher specific impulse and thrust but the required power system and thruster make it unattractive for use in small satellites at volumes less than 6U.

Observations and Testing

The lanthanated tungsten rod was initially chosen to conduct testing. The arc gap was controlled by measuring zero electrical resistance between the cathode and anode. Spacers were placed in front of the first ceramic washer to set the offset. During attempts to initiate the arc, it was found that the system would electrically short after a couple of

seconds of the high voltage pulses. After resetting the system and ensuring the two electrodes were separated from each other, the test was repeated. If the arc gap was set too low the system would quickly short without generating an arc. Figure 24 show pitting and deposition on the tungsten cathode. This material transfer resulted in the electrodes coming into contact during arc initiation.

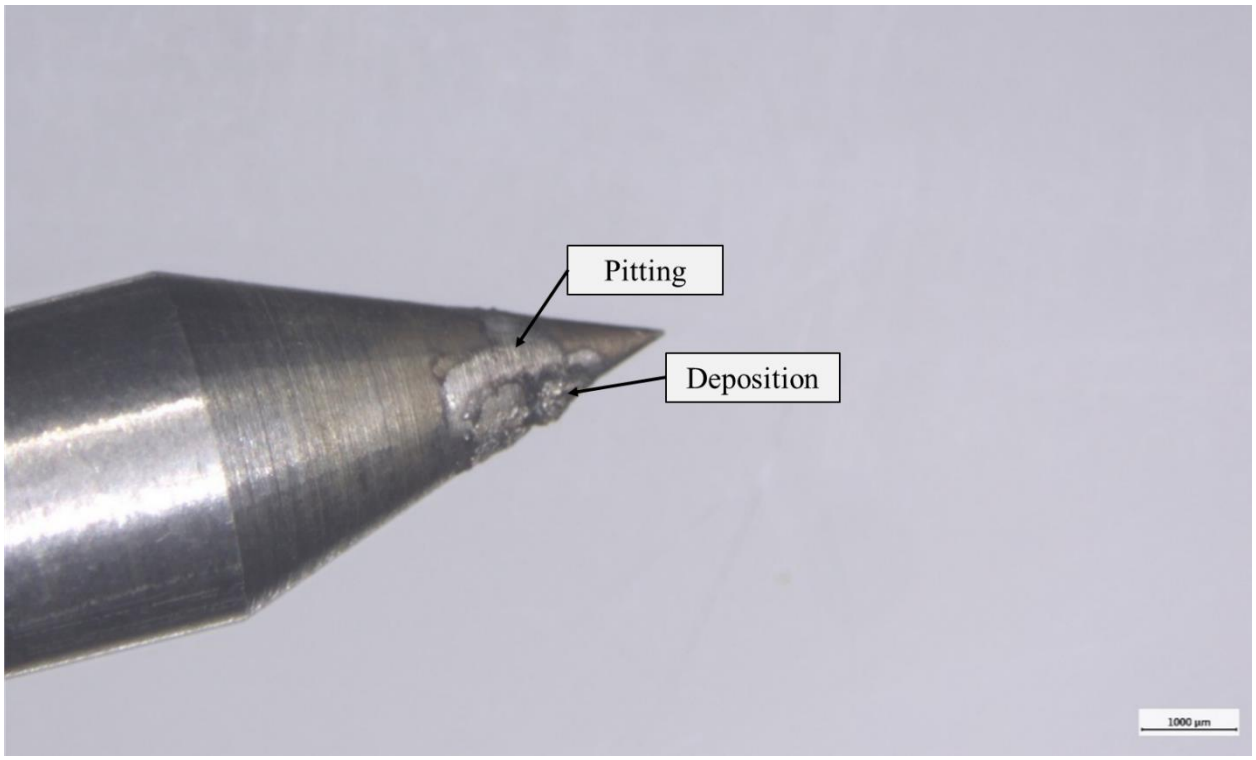

Figure 23 Lanthanated Rod

Figure 24 Lanthanated Rod

Pitting or erosion can be seen on the two figures above as a brighter mark on the surface of the tapered rod. Deposition on the rod is noted by the small protrusions evident in the second figure. Arc transfer was achieved when the cathode had been offset from the anode by at least one millimeter. Arc transfer was confirmed by monitoring the amperage output from the Pro-Fusion power supply. Initial spacing was done under atmospheric conditions without allowing the propellant to flow. Once the arc was generated, propellant was allowed to flow. The result was a small amount of steam generated, and then the arc was blown out while water dripped out the nozzle of the arcjet. After drying the system and resetting the test it was observed that when the cathode and anode were brought into contact with each other, they did not form a closed

circuit. Observations of the converging portion of the nozzle showed an orange discoloration. Tungsten oxide (WO_3) is cited as being a yellow powder [28] and could account for the discoloration in the diverging portion of the nozzle. A new core was installed along with a pure tungsten rod to reduce the potential for corrosion from the lanthanated rod. Pitting and deposition were also observed on the pure tungsten rods as shown in Figure 25 Pure Tungsten Rod

Figure 25 Pure Tungsten Rod

Next, the system was tested to determine if an arc could be struck during vacuum operation. The arc was unable to form between the cathode to the anode during vacuum operation at pressures around 70 millitorr. A faint glow was observed at the connection from the cathode to the power supply with occasional brighter flashes of light. Additional insulators were made to electrically insulate the cathode from the anode. The connection

was changed from a ring terminal connection to a copper tube that was fitted over the cathode from the power supply. Flashing was still observed at the rear of the cathode and was unable to be corrected. Most other arcjet systems strike the arc once the propellant has begun to flow past the cathode [10], [12], [14], [17], [29]–[31]. This reduces the breakdown voltage required for the arc to transfer from the cathode to the anode. Thrust testing was undertaken with the electrode offset of 1.03 millimeters. The external tank provided a constant pressure for a uniform mass flow through the activated valves. Once the pressure in the chamber rose slightly the electrical system was activated to initiate the arc.

During preparation for thrust testing, a leak was discovered in the valving assembly sealing epoxy that, under pressure, resulted in the loss of the tank propellant. Epoxy was reapplied to cover the leak and the propellant tank refilled. The chamber was pumped down to 120 millitorr and the tank pressure set to 30 psig. Once the valves were opened, the arc was initiated without resulting in an arc transfer. Measurements from the thrust stand load cell and tank pressure are shown in Figure 26.

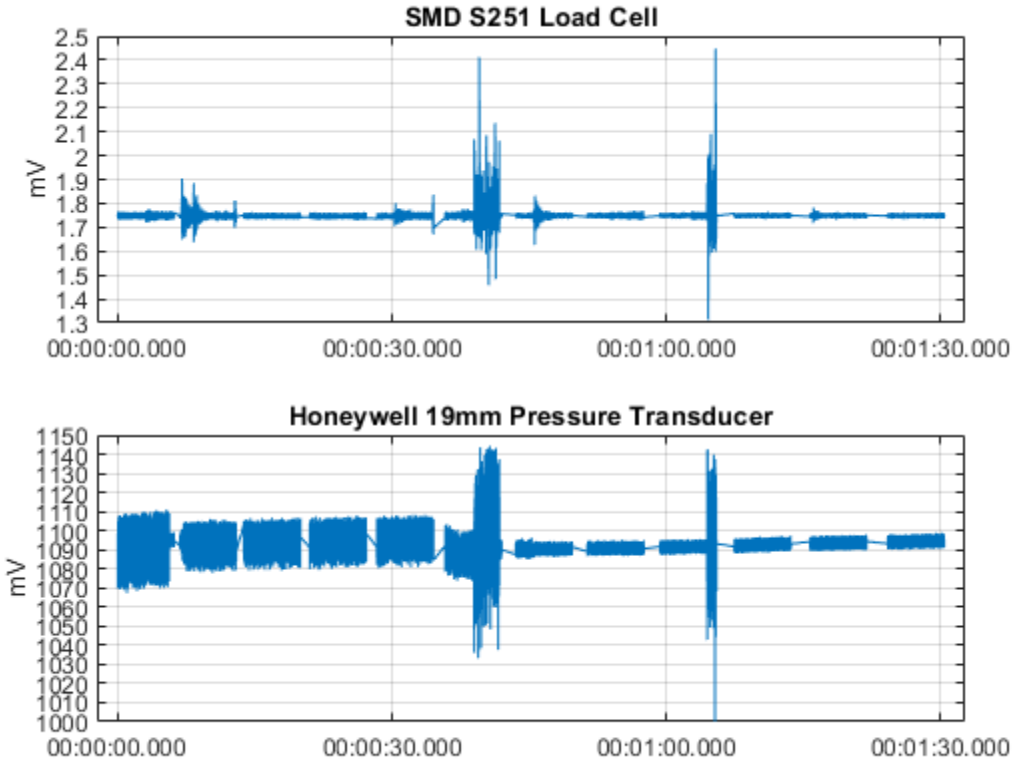

Figure 26 Load and Pressure Output

There are two distinct locations at 39 seconds and past the 1-minute mark that have large spikes in the measured data. These spikes coincide with locations where pressure spikes are also recorded. These points correspond to the activation of the Pro-Fusion microarc power supply. The high voltage input for initiating the arc generated electromagnetic interference (EMI) in the sensor lines. Looking closer at these locations show the definitive repeating nature at these locations.

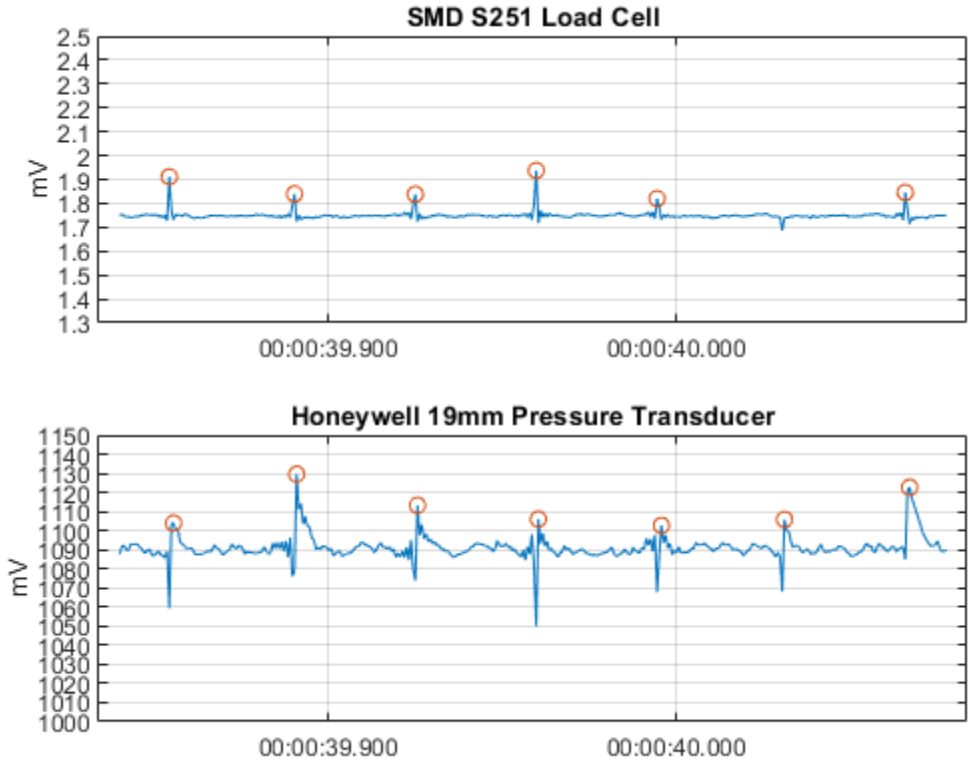

Figure 27 Load Cell and Pressure Closeup

The spikes occur with at a repetition rate of 28 to 29 Hz over the two seconds during the power supply's attempt to generate the electrical arc. This behavior is consistent with the pulsing nature described in the microarc specifications for arc ignition though at double the pulse rate. The load cell output peak correlates to a load of 382 mN. This indicates that electrical shielding of either the sensor or power lines is needed. The electrical interference is generating a reading that is expected to mask the electrical output from the load cell when thrust is produced.

Summary

Arcjets have the potential to produce greater thrust, specific impulse, and Δv than cold gas or resistojet systems. Analysis of the arcjet indicates that the system is

unattractive for satellites smaller than 6U. Much of the space and mass budget for nano- and microsatellites would be consumed by the more complex power system. Pitting of the tungsten rods and corrosion of the nozzle was noted raising concerns about the survivability and reliability of the system for long periods of time. Thrust measurements for the system implied that little to no thrust was produced or was lost amid the EMI.

V. Conclusions and Recommendations

Chapter Overview

Conclusion from the research undertaken is covered along with recommendations for future research. The analytical work suggests that other electrothermal systems are better suited for flight conditions of nanosatellites. Future work needs to be done to refine the tank. Issues with the tank impacted the testing of the system and made corrections difficult.

Conclusions of Research

Theoretically the arcjet system could achieve greater specific impulse, thrust, and Δv levels than those possible for resistojet systems. However, arcjets require more complex power systems. Using water as the propellant in the arcjet operation likely enhanced the corrosion of the electrodes. Methods for mitigating these issues negate the benefits for choosing water as a propellant. A shielding gas to protect the Tungsten anode would reintroduce the hazards of a pressurized container in the secondary payload. Increasing the propellant mass fraction or simply increasing the mass of propellant would produce a larger increase in the system's ΔV. Arcjets require proper spacing of the electrode gap to ensure arc ignition. As the system operates the arc introduces large thermal loads and transfers material between the electrodes. This transfer results in either the electrical shorting of the system or an open circuit. These issues are more complex to solve than the difficulties apparent in a simple electrical heating of water in a resistojet

system. These findings indicate that arcjet systems may not be well suited for use in nano- or microsatellite use.

Recommendations for Future Research

The tank assembly needs refinement to account for the issues encountered during the testing and experimentation. The valve assembly system leaked water under pressure. A refill port allowed for the piston to be reset but made refilling the tank difficult. The passage leading from the refill port to the rest of the tank is small enough that trapped air inside the cylinder prevents unpressurized water from entering the tank. The tank needs to be able to vent air that is trapped inside the container when resetting the cylinder. It is recommended that the refill port be built into the bottom face of the tank. This allows for the visual confirmation of the piston position and the ability to directly refill the tank for further testing without removing the lid and piston.

Aspects of the arcjet system should also be changed to improve testing and performance. A larger expansion ratio with a double angle expansion would improve even the cold gas performance of the system.

Electromagnetic interference prevented the measure of meaningful thrust in the system. Additional insulation and shielding of the power lines for the cathode and anode are needed to reduce the amount of electrical interference during testing.

Summary

The goal of the research was to investigate the use of an arcjet propulsion system for nano- and microsatellites. Other electrothermal systems such as resistojets offer a simpler and more reliable propulsion device at the cost of reduced specific impulse.

Water, while nontoxic and safe, erodes the electrodes if present in large quantities. Mitigating these problems would negate the benefits of choosing water as the propellant for an arcjet system.

Appendix

Table 7 Thrust Calibration Data Points

Mass (kg)	Force (N)	S251 Output (mV)
0.0000	0.0000	1.658014
10.1961	0.1000	1.709155
23.5575	0.2311	1.782539
36.9189	0.3622	1.852158
50.2803	0.4932	1.921572
63.6417	0.6243	1.994391
77.0031	0.7554	2.055389
90.3645	0.8865	2.116581
103.7259	1.0176	2.188943
117.0873	1.1486	2.259455
103.7259	1.0176	2.192914
90.3645	0.8865	2.110782
77.0031	0.7554	2.062059
63.6417	0.6243	2.003321
50.2803	0.4932	1.937706
36.9189	0.3622	1.869290
23.5575	0.2311	1.785314
10.1961	0.1000	1.722823
0.0000	0.0000	1.673351

MATLAB Code for Simplified Arcjet Analysis

```
close all; clear all; clc;
set(0,'defaulttextinterpreter','latex')
```

Constants

```
y=1.33;                                                    %(H2O)
Ratio of Specific Heats for Water Thermodynamic Tables to Accompany Modern
Engineering Thermodynamics
cp=1.867*1e3;                                              %(H2O)(J/kg-K)
Constant Pressure specific heat
a=0.08;                                                    %(H2O) (Si/m/K)
Value for Water from Graph Estimate linear in Nature below "Thermophysical
Properties of H2O-Ar Plasmas"
k=0.0184;                                                  %(H2O) (W/m/K)
Thermal Conductivity of Water Vapor NIST
R_ug=8314.3;                                               %Universal Gas
Constant
MM=18.016;                                                 %Molar Mass
R_g=461;                                                   %Specific Gas
Constant (J/kg/K)
g=9.81;                                                    %(m/s^2)
Acceleration Constant




To=273+25;                                                 %(K) Saturation
Temperature of Steam at P1 Pressure
Te=5000;                                                   %(K) Arc Edge
Temperature
Tw=To;                                                     %(K) Buffer Gas
Temperature


P=200;                                                     %(W) Power
Limitation
Vanode=25;                                                 %(V) Anode
Estimated Voltage Drop
Vcathode=25;                                               %(V) Cathode
Estimated Voltage Drop
I=2;
theta=15;
xatt=3.7*1e-3;                                               %(m) Estimated
attachment downstream


R=1*1e-3;                                                  %(m) Constrictor
Radius
```

```
L=10*1e-3;                                              %(m) Constrictor
Length
mdot=50*1e-6;                                           %(kg/s) Mass Flow
Rate



Iref=pi*R*sqrt(2*a*k)*(Te-Tw);                          %(A) Reference
Current
Istar=I/Iref;                                           %Non
Dimensionalized Current
xref=(mdot*cp/(2*pi*k))*sqrt(Tw/Te);                    %(m) Reference
Length
xstarL=L/xref;                                          %Non-
Dimensionalized Length at Constrictor End
syms ra
FUN=log(sqrt((1+ra)/(1-ra)))-ra;
r_a=double(vpasolve(FUN==xstarL*Istar,[0 1]));          %Non-
Dimensionalized Arc Radius at Constrictor End
mdotstar=1-r_a^2;                                       %Non-
Dimensionalized Mass Flow
mdotref=mdot/mdotstar;                                  %(kg/s) Reference
Mass FLow
syms p1
FUN=sqrt(y)*((2/(y+1))^((y+1)/(2*(y-1))))*(p1*pi*R^2)/sqrt(R_g*Tw);
P1=double(vpasolve(FUN==mdotref));                      %(Pa) Chamber
Pressure
syms M
ER=(1/M)*((1+0.5*(y-1)*M^2)/(1+0.5*(y-1)))^((y+1)/(2*(y-1)));
M=double(vpasolve(ER==4,[1 inf]));                      %Exit Mach Number
Pe=P1/(1+(y-1)*M^2/2)^(y/(y-1));                        %(Pa) Exit
Pressure
Ae=pi*(R^2)*4;                                          %(m^2) Exit Area
Thrust=Pe*Ae*(1+y*M^2);                                 %(N) Thrust
Isp=Thrust/(mdot*g);                                    %(s) Specific
Impulse
Eref=2*sqrt(2*k/a)/R;                                   %(V/m) Reference
Electric Field
Vconst=Eref*xref*(1/(2*Istar))*log(1/(1-r_a^2));        %(V) Constrictor
Voltage Drop
R_att=R+xatt*tand(theta);                               %(m) Estimated Arc
Attachment
Vnozzle=2*sqrt(2*k/a)*(1/(r_a*tand(theta)))*log(R_att/R);%(V) Nozzle
Voltage Drop
Vtotal=20+20+Vconst+Vnozzle;                            %(V) Total
Voltage Drop
```

```
P=I*Vtotal;                                                    %(W) Power
Required
JetPower=Thrust*Isp*g/2;                                       %(W) Thrust Power
eta=JetPower/P;                                                %Efficiency


data=[Thrust Isp P JetPower eta]'
fprintf('Thrust:\t\t%.3f N\nIsp:\t\t%.3f s\nPower:\t\t%.3f
W\nJetPower:\t%.3f W\nEfficiency:\t%.3f',data)
```

MATLAB Code for Electrothermal Analysis

```
close all; clear all; clc;
set(0,'defaulttextinterpreter','tex')


tp=[0.5 1 6]*3600;
alpha=46;
eta=0.3;


minmassfraction=[0.1 0.3 0.8];


for i=1:length(tp)
    figure
comparison(tp(i),alpha,eta,minmassfraction(i))
end
```

```
function comparison(tp,alpha,eta,minmassfraction)
```

Constants

```
g=9.81;             %m/s^2
m=10;




n=100;
Ispmin=40;
Ispmax=210;
```

```
%minmassfraction=0.8;
maxmassfraction=1;
%tp=3600*6;


Isp=linspace(Ispmin,Ispmax,n);
Du=[10:10:50];


MPR=10/(10-0.246);
Ispreq=Du./(g*log(MPR));


str=[];
linS={'-b','--b',':b','-.b','-+b','-xb','-ob'};
for i=1:length(Du)


    du=Du(i);
    v=g.*Isp;
    vc=sqrt(2*alpha*tp*eta);
    MR=(exp(du./v)./(1-(exp(du./v)-1).*v.^2./vc^2)).^(-1);
    idx=find(Isp>=Ispreq(i));


    if MR(idx(1))>minmassfraction
        state='on';
    else
        state='off';
    end


    hold on;grid on;
    plot(Isp(idx),MR(idx),linS{i},'HandleVisibility',state)




    if MR(idx(1))>minmassfraction
        str=[str append(string(du),' m/s')];
    else
    end


end
```

```
axis([Ispmin Ispmax minmassfraction maxmassfraction])
xlabel('Specific Impulse (s)')



vreq=ones([1 length(Ispreq)]);
PMR=ones([1 length(Ispreq)]);
for i=1:length(Ispreq)
    du=Du(i);
    vreq(i)=g.*Ispreq(i);
    v=vreq(i);
    vc=sqrt(2*alpha*tp*eta);
    PMR(i)=(exp(du./v)./(1-(exp(du./v)-1).*v.^2./vc^2)).^(-1);
end



plot(Ispreq,PMR,'--k','HandleVisibility',"on")
str=[str append('Isp Limit')];
ylabel('Payload Mass Fraction')



title(['t_{b}=' num2str(tp/3600) ' hrs, \alpha=' ...
    num2str(alpha) ' W/kg, ' '\eta_{t}=' num2str(eta)])
legend(str,'Location',"bestoutside")



end
```

Bibliography

[1] C. B. Bok, A. Comeau, A. Dolgopolov, T. Halt, C. Juang, and P. Smith, “Smallsats by the Numbers,” 2020. Accessed: May 10, 2021. [Online]. Available: https://brycetech.com/reports/report-documents/Bryce_Smallsats_2020.pdf

[2] D. Krejci and P. Lozano, “Space Propulsion Technology for Small Spacecraft,” *Proceedings of the IEEE*, vol. 106, no. 3, pp. 362–378, Mar. 2018, doi: 10.1109/JPROC.2017.2778747.

[3] NASA, “State of the Art of Small Spacecraft Technology,” Moffet Field, Oct. 2020. Accessed: Sep. 06, 2021. [Online]. Available: http://www.nasa.gov/smallsat-institute/sst-soa

[4] J. Mueller, J. Ziemer, and R. Hofer, “Survey of Propulsion Technologies Applicable to Cubesats,” *Joint Army-Navy-NASA-Air Force (JANNAF), Colorado Springs, Colorado, May 3, 2010*. NASA Center for Aerospace Information (CASI), United States, May 03, 2010.

[5] G. P. Sutton and O. Biblarz, “Rocket Propulsion Elements,” in *Rocket Propulsion Elements*, 9th. ed., Hoboken: John Wiley & Sons, Inc., 2017, pp. 654–658.

[6] NASA, “State-of-the-Art of Small Spacecraft Technology,” Moffet Field, Oct. 2021. Accessed: Jan. 13, 2022. [Online]. Available: http://www.nasa.gov/smallsat-institute/sst-soa

[7] J. R. Wertz, D. F. Everett, and J. J. Puschell, Eds., *Space Mission Engineering*, Third Prin. Torrance: Microcosm Press, 2018.

[8] N. Roney, F. Llados, S. S. Little, and D. B. Knaebel, “TOXICOLOGICAL PROFILE FOR AMMONIA,” Atlanta, Georgia, 2004.

[9] G. Choudhary, H. Ilansen, S. Donkin, and C. Kirman, “TOXICOLOGICAL PROFILE FOR HYDRAZINE,” Atlanta, Georgia, 1997.

[10] Y. Yamamoto and T. Tachibana, “Performance Characteristics of a Water/Dimethyl-Ether Propellant Arcjet,” *Journal of Propulsion and Power*, vol. 36, no. 4, pp. 639–641, May 2020, doi: 10.2514/1.B37730.

[11] N. Yanagida and H. Horisawa, “Al-water Fed Chemically Augmented DC Arcjet Characteristics,” in *50th AIAA/ASME/SAE/ASEE Joint Propulsion Conference*, American Institute of Aeronautics and Astronautics, 2014. doi: doi:10.2514/6.2014-3504.

[12] F. Inoue and H. Tahara, “Performance Characteristics of Low-Power Arcjet Thrusters Using Green Propellants of HAN and Water,” in *50th AIAA/ASME/SAE/ASEE Joint Propulsion Conference*, American Institute of Aeronautics and Astronautics, 2014. doi: doi:10.2514/6.2014-3506.

[13] B. Wollenhaupt, Q. H. Le, and G. Herdrich, “Overview of thermal arcjet thruster development,” *Aircraft Engineering and Aerospace Technology*, vol. 90, no. 2, pp. 280–301, Mar. 2018, doi: 10.1108/AEAT-08-2016-0124.

[14] F. M. Curran and J. M. Sankovic, “A Low-Erosion Starting Technique for High-Performance Arcjets,” *Joint Propulsion Conference*. NASA Center for Aerospace Information (CASI), United States, Sep. 01, 1994. [Online]. Available: https://afit.idm.oclc.org/login?url=https://search.ebscohost.com/login.aspx?direct=true&db=edsnas&AN=edsnas.19950006934&site=eds-live

[15] E. S. Huston and J. R. Stone, “The NASA/USAF arcjet research and technology program.” NASA Center for Aerospace Information (CASI), United States, Jan.

01, 1987. [Online]. Available: https://afit.idm.oclc.org/login?url=https://search.ebscohost.com/login.aspx?direct=true&db=edsnas&AN=edsnas.19870015092&site=eds-live

[16] J. Sankovic and J. Hopkins, “Miniaturized arcjet performance improvement,” in *32nd Joint Propulsion Conference and Exhibit*, American Institute of Aeronautics and Astronautics, 1996. doi: doi:10.2514/6.1996-2962.

[17] J. M. Sankovic and D. T. Jacobson, “Performance of a Miniaturized Arcjet,” *NASA TM-107062*. NASA, Cleveland, Jul. 1995. Accessed: Nov. 20, 2021. [Online]. Available: https://ntrs.nasa.gov/api/citations/19960008160/downloads/19960008160.pdf

[18] G. Hartsfield, Carl R., Shelton,Travis, Cobb, “Design of a High Reliability Compact CubeSat Propulsion System.” p. 9, 2021. doi: 10.2514/6.SCITECH.

[19] M. Sammons, “Guidelines for tungsten electrodes: An Update,” *The FABRICATOR*, Apr. 28, 2021. https://www.thefabricator.com/thewelder/article/consumables/guidelines-for-tungsten-electrodes-an-update (accessed Jan. 27, 2022).

[20] J. HAMLEY and J. SANKOVIC, “A soft-start circuit for arcjet ignition,” in *29th Joint Propulsion Conference and Exhibit*, American Institute of Aeronautics and Astronautics, 1993. doi: doi:10.2514/6.1993-2396.

[21] E. & Hall, “Pro-Fusion Dual Arc 82 HFP Micro-Arc Power Supply Your Trusted Partner in Precision Welding”, Accessed: Jan. 27, 2022. [Online]. Available: www.pro-fusiononline.com

[22] M. MARTINEZ-SANCHEZ and A. SAKAMOTO, “Simplified analysis of arcjet thrusters,” in *29th Joint Propulsion Conference and Exhibit*, Jun. 1993, p. 17. doi: 10.2514/6.1993-1904.

[23] R. Balmer, *Thermodynamic Tables to Accompany Modern Engineering Thermodynamics*. Elsevier Ltd, 2011.

[24] P. Křenek, “Thermophysical Properties of H2O–Ar Plasmas at Temperatures 400–50,000 K and Pressure 0.1 MPa,” *Plasma Chemistry and Plasma Processing*, vol. 28, no. 1, p. 107, 2008, doi: 10.1007/s11090-007-9113-z.

[25] M. Huber, “THERMAL CONDUCTIVITY OF GASES,” CRC Handbook of Chemistry and Physics, CRC Press, Boca Raton, FL, 2019. [Online]. Available: https://tsapps.nist.gov/publication/get_pdf.cfm?pub_id=926438

[26] R. G. Jahn, *Physics of Electric Propulsion*. Mineola: Dover Publications, 1968.

[27] L. R. Piänero and G. E. Bowers, *Power electronics for a miniaturized arcjet / Luis R. Piänero and Glen E. Bowers.* 1997. [Online]. Available: https://afit.idm.oclc.org/login?url=https://search.ebscohost.com/login.aspx?direct=true&db=edsgpr&AN=edsgpr.000997254&site=eds-live

[28] H. Guzmán, M. A. Farkhondehfal, K. R. Tolod, S. Hernández, and N. Russo, “Photo/electrocatalytic hydrogen exploitation for CO2 reduction toward solar fuels production,” *Solar Hydrogen Production: Processes, Systems and Technologies*, pp. 365–418, Jan. 2019, doi: 10.1016/B978-0-12-814853-2.00011-4.

[29] J. Czika Jr and L. E. Wallner, “Arc-jet thrustor for space propulsion.” NASA Center for Aerospace Information (CASI), United States, Jun. 01, 1965. [Online]. Available:

https://afit.idm.oclc.org/login?url=https://search.ebscohost.com/login.aspx?direct=true&db=edsnas&AN=edsnas.19650017046&site=eds-live

[30] F. CURRAN and C. SARMIENTO, “Low power arcjet performance,” in *21st International Electric Propulsion Conference*, American Institute of Aeronautics and Astronautics, 1990. doi: doi:10.2514/6.1990-2578.

[31] F. CURRAN, S. BULLOCK, T. HAAG, CHARLESJ. SARMIENTO, and J. SANKOVIC, “Medium power hydrogen arcjet performance,” in *27th Joint Propulsion Conference*, American Institute of Aeronautics and Astronautics, 1991. doi: doi:10.2514/6.1991-2227.

REPORT DOCUMENTATION PAGE

Form Approved
OMB No. 074-0188

1. REPORT DATE *(DD-MM-YYYY)*	2. REPORT TYPE	3. DATES COVERED *(From – To)*
11-02-2022	Master's Thesis	March 2021 – March 2022

TITLE AND SUBTITLE

DESIGN OF AN ELECTRO-THERMAL NANO- AND MICROSATELLITE PROPULSION SYSTEM

5a. CONTRACT NUMBER

5b. GRANT NUMBER

5c. PROGRAM ELEMENT NUMBER

5d. PROJECT NUMBER

5e. TASK NUMBER

5f. WORK UNIT NUMBER

6. AUTHOR(S)

Founds, James H., Captain, USSF

7. PERFORMING ORGANIZATION NAMES(S) AND ADDRESS(S)
Air Force Institute of Technology
Graduate School of Engineering and Management (AFIT/EN)
2950 Hobson Way, Building 640
WPAFB OH 45433-7765

8. PERFORMING ORGANIZATION REPORT NUMBER

AFIT-ENY-MS-22-M-291

9. SPONSORING/MONITORING AGENCY NAME(S) AND ADDRESS(ES)
Intentionally left blank

10. SPONSOR/MONITOR'S ACRONYM(S)

11. SPONSOR/MONITOR'S REPORT NUMBER(S)

12. DISTRIBUTION/AVAILABILITY STATEMENT
DISTRUBTION STATEMENT A. APPROVED FOR PUBLIC RELEASE; DISTRIBUTION UNLIMITED.

13. SUPPLEMENTARY NOTES
This material is declared a work of the U.S. Government and is not subject to copyright protection in the United States.

14. ABSTRACT

This research focused on designing an arcjet system with water as the propellant. Previous research developed a compact, reliable, and safe propellant storage and feed system. The goal is to combine the arcjet with the previous tank to achieve thrust and specific impulse characteristics greater than cold gas or resistojet system. This platform features a 1U, non-hazardous, and sub-kilowatt powered propulsion system for nanosatellites. A simplified analysis of the design predicts thrust and specific impulse greater than can be achieved by cold gas or resistojet thrusters. Testing resulted in oxidation of the electrodes raising concerns about the longevity of the system. Oxidation reduced the reliability of arc initiation in vacuum and negligible thrust measurements. Similar systems resolution to these issues make the system suboptimal for nanosatellite implementation

15. SUBJECT TERMS
Space Propulsion

16. SECURITY CLASSIFICATION OF:			17. LIMITATION OF ABSTRACT	18. NUMBER OF PAGES	19a. NAME OF RESPONSIBLE PERSON
a. REPORT	b. ABSTRACT	c. THIS PAGE			Dr. Carl R. Hartsfield, AFIT/ENY
U	U	U	UU	69	19b. TELEPHONE NUMBER *(Include area code)* (937) 255-6565, ext 4667 (NOT DSN) (carl.hartsfield@afit.edu)

Standard Form 298 (Rev. 8-98)
Prescribed by ANSI Std. Z39-18